MASTER THESIS

FATIGUE LIFE OF 1045 STEEL WITH AN ARTIFICIAL SMALL DEFECT: EXPERIMENTS AND MODELING BASED ON SMALL CRACK GROWTH

NATHALIA MANES SANTOS

Brasília, December 14th, 2023

UNIVERSITY OF BRASÍLIA

FACULTY OF TECHNOLOGY

DEPARTMENT OF MECHANICAL ENGINEERING

UNIVERSITY OF BRASÍLIA
Faculty of Technology
Department of Mechanical Engineering

FATIGUE LIFE OF 1045 STEEL WITH AN ARTIFICIAL SMALL DEFECT: EXPERIMENTS AND MODELING BASED ON SMALL CRACK GROWTH

NATHALIA MANES SANTOS

REPORT SUBMITTED TO THE DEPARTMENT OF MECHANICAL ENGINEERING OF THE FACULTY OF TECHNOLOGY OF THE UNIVERSITY OF BRASÍLIA AS A PARTIAL REQUIREMENT FOR OBTAINING THE DEGREE OF MASTER IN MECHANICAL SCIENCES.

APPROVED BY:

_____
Prof. Fábio Comes de Castro, D.Sc. (ENM/UnB)
(Committee Chair)

_____
Prof. Jorge Luiz de Almeida Ferreira, D.Sc. (ENM/UnB)
(Committee Member)

_____
Prof. Waldek Wladimir Bose Filho, D.Sc. (EESC/USP)
(Committee Member)

Brasília/DF, December 14th, 2023.

CATALOG SHEET

SANTOS, NATHALIA MANES

Fatigue life of 1045 steel with an artificial small defect: Experiments and modeling based on small crack growth.

[Federal District] 2023.

xi, 47 p., 210 x 297 mm (ENM/FT/UnB, Master, Mechanical Science, 2023)

Master Thesis – University of Brasília.

Faculty of Technology.

Department of Mechanical Engineering.

1. Fatigue life
2. Microdefects
3. 1045 Steel
4. Small Crack Gowth Model

I. ENM/FT/UnB

II. ENM.DM-__/2023

REFERENCE

SANTOS, N. M., (2023) Fatigue life 1045 steel with an artificial small defect: Experiments and modeling based on small crack growth. Master Thesis, Publication ENM.DM-__/2021, Department of Mechanical Engineering, University of Brasília, DF, 47 p.

ASSIGNEMENT OF RIGHTS

AUTHOR: Nathalia Manes Santos.

TÍTULO: Fatigue life 1045 steel with an artificial small defect: Experiments and modeling based on small crack growth.

DEGREE: Master YEAR: 2023

_____

Nathalia Manes Santos

E-mail: nath.manes@gmail.com

ACKNOWLEDGMENT

To God, my Lord, and Savior, who called me out of darkness into His marvelous light. I will never be worthy of such grace.

To my parents, Sheila and Eduardo. They supported me in every phase of my life and were by my side during this project. I don't think I will ever retribute all the favors you did for me, but I hope to honor you and your efforts for me and my sister. I thank my sister, Mariana, one of my greatest friends. She has been there for me all my life. I owe this family so much, and I know I can count on them anytime.

To my supervisor, professor Fábio, whose guidance was essential for the conclusion of this work. He patiently taught me so much, and I thank him for his support during this study. Learning from him was a great blessing and opportunity.

To the professors from the Industrial Engineering Department and the Mechanical Sciences Undergraduate Program of the University of Brasília who were part of my academic journey.

To all my friends from Semear Presbyterian Church. To all my colleagues that I knew during graduation time. To all the important people in my life.

To my labmates, Karoline, Natália, Andre, Giorgio, Rodrigo, Roberto, Felipe, and Lucas. Thank you all for your help with this research as well as the assistance with the course of the disciplines, and, of course, the good times that we spent together.

For from Him and through Him and to Him are all things. To Him be glory forever. Amen. (Romans 11:36)

ABSTRACT

A major portion of the fatigue life of materials consists of the growth of small cracks. Despite the progress in understanding small fatigue crack growth over the last 50 years, it remains a fundamental and active research topic in fatigue. In this context, the aims of the present work were twofold: (i) to experimentally characterize the small crack growth of SAE 1045 carbon steel with a small surface defect when subjected to cyclic loading and (ii) to assess the accuracy of small crack growth models in predicting fatigue life. Cylindrical specimens with an artificial cylindrical hole (diameter and depth of 400 μm) were subjected to cyclic axial loading under load ratios of -1 and 0.1. The tests were conducted in the high-cycle fatigue regime, with lives ranging from 10^4 to 10^7 cycles. Crack growth in the vicinity of the hole was monitored by periodically interrupting the tests and measuring the crack length using a confocal laser microscope. The incremental polynomial method was then used to obtain the crack growth rate vs. crack length. A modified form of the Fatemi model for small crack growth rate was developed by substituting the Smith–Watson–Topper parameter for a Walker-type parameter. The constants of the model were determined by fitting the small crack growth data obtained under uniaxial loading. To verify the accuracy of fatigue life predictions under multiaxial loading, axial/torsional test data previously produced by the Fatigue, Fracture, and Materials research group of the University of Brasília were used. The data included in-phase and out-of-phase loading conditions and the presence of mean stress. It was demonstrated that using the Walker-type parameter yielded improved life estimates, especially for the tests involving mean stress. Most of the fatigue life estimates were within a factor of 3 with respect to the measured lives.

RESUMO

Vida à fadiga do aço 1045 com um microdefeito artificial: Experimentos e modelagem baseada em crescimento de trincas pequenas

Uma parte significativa da vida à fadiga dos materiais consiste no crescimento de pequenas trincas. Apesar do progresso na compreensão do crescimento de pequenas trincas de fadiga nos últimos 50 anos, ainda é um tema fundamental e ativo na pesquisa de fadiga. Nesse contexto, os objetivos do presente trabalho foram: (i) caracterizar experimentalmente o crescimento de pequenas trincas em aço carbono SAE 1045 com um pequeno defeito superficial quando submetido a carga cíclica e (ii) avaliar a precisão dos modelos de crescimento de pequenas trincas na previsão da vida útil à fadiga. Amostras cilíndricas com um furo cilíndrico artificial (com diâmetro e profundidade de 400 μm) foram submetidas a carga axial cíclica sob razões de carga de -1 e 0.1. Os testes foram conduzidos no regime de fadiga de alto ciclo, com vidas variando de 10^4 a 10^7 ciclos. O crescimento da trinca nas proximidades do furo foi monitorado interrompendo periodicamente os testes e medindo o comprimento da trinca usando um microscópio confocal à laser. O método polinomial incremental foi então utilizado para obter a taxa de crescimento da trinca em relação ao seu comprimento. Uma forma modificada do modelo de Fatemi para a taxa de crescimento de pequenas trincas foi desenvolvida substituindo o parâmetro Smith–Watson–Topper por um parâmetro do tipo Walker. As constantes do modelo foram determinadas ajustando os dados de crescimento de trincas obtidos sob carga uniaxial. Para verificar a precisão das previsões de vida útil à fadiga sob carga multiaxial, foram utilizados dados de teste axial/torcional previamente produzidos pelo grupo de pesquisa em Fadiga, Fratura e Materiais da Universidade de Brasília. Os dados incluíam condições de carga em fase e fora de fase, assim como a presença de tensão média. Foi demonstrado que o uso do parâmetro do tipo Walker proporcionou estimativas de vida útil aprimoradas, especialmente para os testes envolvendo tensão média. A maioria das estimativas de vida à fadiga estava dentro de um fator de 3 em relação às vidas medidas.

SUMMARY

LIST OF FIGURES

LIST OF TABLES

LIST OF SYMBOLS

N_{t}	total fatigue life
N_{i}	number of cycles to crack initiation
N_{lc}	number of cycles for a long crack propagation
N_{nuc}	number of cycles to crack nucleation
N_{mcg}	number of cycles for microstructurally small crack growth
N_{scg}	number of cycles for physically small crack growth
ΔK	stress intensity factor range
ΔK_{th}	threshold stress intensity factor range
R	load ratio
E	Young's modulus
σ_{m}	material property
σ_{y}	monotonic yield stress
σ_{u}	ultimate tensile strength
σ_{a}	stress amplitude
σ_{xa}	normal stress amplitude
σ_{xm}	mean stress
σ_{max}	maximum stress
$\sigma_{\mathrm{n,max}}$	maximum normal stress
$\varepsilon_{\mathrm{na}}$	normal strain amplitude
$\varepsilon_{\mathrm{max}}$	maximum remote strain
$\varepsilon_{1,\mathrm{a}}$	maximum principal strain on the plane with maximum principal stress
l	total crack length

l_i	initial crack length
l_f	final crack length
l_L	left crack length
l_R	right crack length
N_i	a specific number of cycles
l_i	a specific crack length
$\hat{l}_i$	crack length when $N = N_i$ in the Incremental Polynomial Method
n	number of points determination parameter for Incremental Polynomial Method
b_0, b_1, b_2	regression parameter for Incremental Polynomial Method
C_1, C_2	input data scale parameter for Incremental Polynomial Method
$B_{N,} j$	material constants in the Nisitani model
C_N, k	material constants in the Nisitani model
C_F, s, t	material constants in the Fatemi model
n, m, ξ	material constants
FP	fatigue parameter

1. INTRODUCTION

1.1. Motivation

Engineers responsible for the durability analysis of mechanical components under cyclic loads often face concerns regarding fatigue failure. This is a pertinent concern since many component failures occur due to inadequate fatigue design [1]. In this context, the existence of accurate models for fatigue life estimation is of utmost importance for the safe design of components against fatigue.

Fatigue damage is a crack growth process that eventually ends when the crack achieves a critical size at which abrupt fracture occurs. Typically, cracks initiate at the site of the highest local stress/strain within the component. Defects such as non-metallic inclusions, voids, cavities, scratches, internal shrinkage, and corrosion pits act as stress concentrators, increasing the likelihood of crack formation. As a result, the presence of defects decreases the material resistance to fatigue [2]. Given that it is nearly impossible to manufacture a defect-free component, it is crucial to recognize the existence of defects when designing against fatigue failure.

The importance of the small crack growth phase in damage-tolerant approaches to fatigue life prediction is evident in the literature. For instance, in Ref. [3], data of nickel-based superalloys was used to evaluate the difference between life predictions of a typical gas turbine disc based on small and large cracks growth at the cooling hole (Fig. 1.1). The authors concluded that the life prediction based on small crack growth was more conservative within a factor of 2 for lives ranging from 10^3 to 10^5 cycles. In a more recent investigation [4], the total fatigue life of 7075 aluminum alloy was predicted by adding up the number of cycles necessary for crack initiation, small crack growth, and long crack growth.

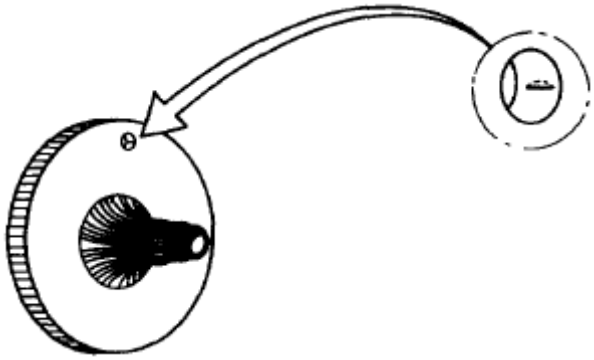

Figure 1.1 - Idealized turbine disc with web cooling hole. The detail shows a semi-elliptical surface crack at the hole (modified from [3]).

To assess the influence of defects on fatigue life, small crack growth models based on a geometric characteristic of the defect, such as its size, have been developed. For instance, in Ref. [5] a small crack growth model based on the porosity size measured on the fracture surface of aluminum alloy was evaluated. The results correlated well with the experimental data. Another research employed a multi-scale crack propagation approach to predict the fatigue life of nickel-based GH4169 alloy specimens containing different initial defect sizes. This approach involved microstructurally small cracks, physically small cracks, and large cracks. The results of this study also agreed well with the experimental data [6].

Murakami [7] recently stated that the mechanics of cracks or defects critically influence the form of the S-N curve. His study aimed to explore the correlation between the S-N curve and the small crack growth in annealed medium carbon steel specimens with various sizes of drilled holes. The author conducted fully reversed fatigue tests and verified a mutual relation between the initial defect size and the S-N curve. Figure 1.2 is a micrograph produced by Murakami, which shows a small crack measuring 392 μm in length emanating from a hole with a diameter and depth of 100 μm.

Figure 1.2 - Crack with a length of 392 µm formed at a hole with a diameter and depth of 100 µm (modified from [7]).

In Ref. [8], a method for fatigue crack growth was employed for life prediction of lifting lugs, which is a crucial component of aerial bombs (Fig. 1.3). The analysis was necessary because the structure failed earlier than expected due to an inclusion defect formed during the casting process, which accelerated the crack propagation. To estimate the fatigue life prediction, the authors divided the life into two phases: small crack growth and long crack growth. The number of cycles required for each stage was estimated based on small and long crack theories. The results indicated that the defect size had a great influence on fatigue life, which was mainly occupied by the small crack growth stage.

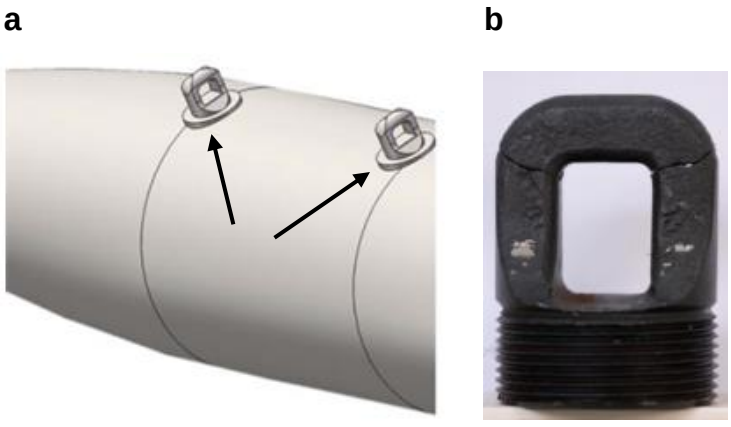

Figure 1.3 - Indication of lifting lugs in an aerial bomb (a) and a failed lifting lug (b) (modified from [8]).

Despite the progress in understanding small fatigue crack growth over the last 50 years, it remains a fundamental and active research topic in fatigue. This research has seen a renewal in interest in recent years due to factors such as (i) the capability of current experimental techniques (e.g., X-ray computed tomography) that can reveal very small flaws in materials, and (ii) fabrication processes such as additive manufacturing that inherently produces materials containing defects. Moreover, the domain of application and accuracy of the existing small crack growth models is not clear due to the limited scope of the fatigue experiments conducted so far.

1.2. Objectives

The general objective of this research was to gain an understanding of fatigue crack growth at small defects in carbon steel and to develop (or improve) a small crack growth approach to life prediction. Within this context, the specific objectives of this work were as follows:

1) To conduct high-cycle uniaxial fatigue tests on SAE 1045 carbon steel with a small blind hole (diameter and depth of 400 μm) under stress ratios of -1 and 0.1, covering lives from 10^4 to 10^7 cycles to failure.
2) To experimentally determine the crack growth rate vs. crack length diagram for the tests mentioned above, using a confocal laser microscope and the incremental polynomial technique.
3) To assess the life estimates of the small crack growth relation proposed by Fatemi [9] using the uniaxial test data produced here and the axial/torsional data previously produced by the Fatigue, Fracture, and Materials research group of the University of Brasília [10].
4) To evaluate the impact on the fatigue life estimates of the Fatemi model when the Smith–Watson–Topper parameter is substituted for a Walker-type parameter.

2. FATIGUE LIFE PREDICTION BASED ON FRACTURE MECHANICS

2.1. The importance of small crack growth in fatigue life prediction

From a fracture mechanics perspective [11–13], fatigue damage is viewed as a process of crack growth over various length scales. During its early stage, the crack grows within a grain and is referred to as a *microstructurally short crack*. When the crack length becomes of the order of a few grains, the crack is usually termed as *physically small crack*. After this stage, the crack length is long enough (say, longer than 100 grains) for the influence of microstructural features on the crack growth rate to become insignificant. During this stage, the crack is often classified as a *long crack*. The final stage occurs when the crack size achieves a critical size in which crack growth occurs abruptly and the component generally breaks into two or more parts. Figure 2.1 illustrates the length scales involved in crack growth.

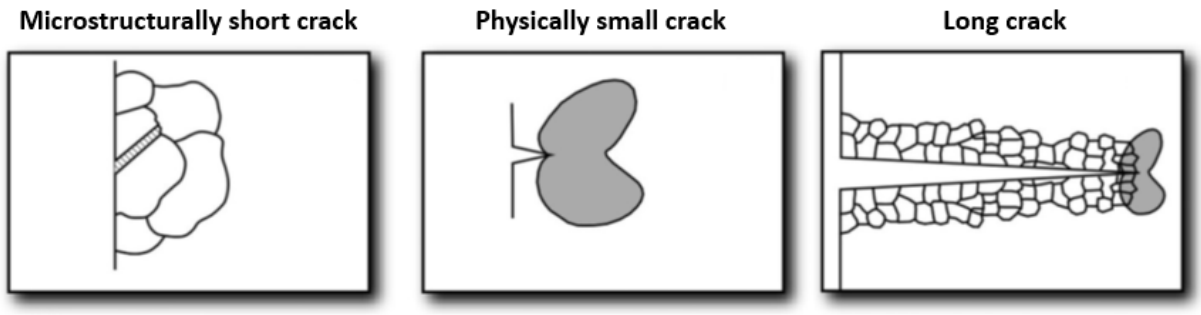

Figure 2.1 - Crack propagation stages (modified from [11]).

The total number of cycles to failure, N_{t}, of a component under cyclic loading is usually decomposed as a sum of two periods: the number of cycles to crack initiation, N_{i}, and the number of cycles for a long crack to propagate to a critical size, N_{lc}. This decomposition may be expressed as:

$$N_{\mathrm{t}} = N_{\mathrm{i}} + N_{\mathrm{lc}} \tag{2.1}$$

Here, the term crack initiation refers to the appearance of a macroscopic (visible) crack on the surface of the component, whose length typically varies from 0.5 to 2 mm. As discussed in Refs. [11,12,14], the separation between crack initiation and propagation stages has only a qualitative nature since a quantitative demarcation between the two stages is ambiguous. However, the split of the total life into two distinct periods is useful for engineering purposes, and it has been widely adopted for assessing the fatigue life of engineering components.

It should be realized that "crack initiation" is not a single event that occurs at a precise number of loading cycles. It is the result of a microscopic crack growth process that culminates in the appearance of a macroscopic crack. It starts with the generation of a crack of a few microns in size, which then propagates through the grain or along a grain boundary. Subsequently, the crack grows at a length scale on the order of a few grains, up to a moment when the crack becomes visible at the macroscopic (millimeter) scale. For detailed discussions on the physics of fatigue crack initiation, the reader is referred to [15,16] and references therein.

Since crack initiation is a succession of crack growth stages over increasingly higher length scales (each one involving different physical mechanisms), attempts have been made [12] to decompose the crack initiation life as

$$N_{\mathrm{i}} = N_{\mathrm{nuc}} + N_{\mathrm{mcg}} + N_{\mathrm{scg}} \tag{2.2}$$

In this expression, N_{nuc} is the number of cycles to nucleate (incubate) a crack. N_{mcg} is the period of growth of a crack with a length comparable to the size of a typical microstructural unit (e.g., a grain in polycrystalline materials). N_{scg} is the number of cycles spent during physically small crack growth. The crack length in this regime, which is typically in the range of 0.5–2 mm, is longer than the microstructural length scale. However, the size of the crack tip plastic zone may violate the small-scale yielding condition and, therefore, the crack growth rate cannot be predicted using LEFM parameters.

Various researchers [12,17–20] have indicated that most of the total life of engineering components and structures under cyclic loading may be spent in small fatigue crack growth. It was also suggested [9] that the period of small crack growth is predominant in materials containing defects. This behavior occurs due to the stress concentration caused by the defect which results in rapid crack formation; therefore, the crack nucleation life can be neglected. Furthermore, the period of long crack growth may be negligible compared with the total fatigue life or is not tolerable depending on the methodology adopted for fatigue design. Due to the importance of the period of small crack growth in fatigue life, researchers have developed models for predicting the small crack growth rate. For uniaxial loading conditions, the contributions made in [19,21–25] are worth mentioning. Recent studies [9] have proposed small crack growth models for multiaxial loading conditions.

A review of small crack growth models for uniaxial and multiaxial loadings will be presented in this chapter. Before that, the next section gives a brief discussion on the characteristic behavior of small fatigue crack growth and on the inadequacy of LEFM parameters in predicting growth rates in this regime.

2.2. Limitation of LEFM in describing small crack growth

The Paris equation [26,27] is widely used to relate the fatigue crack growth rate with the stress intensity factor range. This equation is valid for long cracks under small-scale yielding (i.e., when the crack tip plastic zone is small relative to the crack length). The limitations of Paris' approach for describing small crack growth were first pointed out in the experimental study of Pearson [28] and Kitagawa and Takahashi [18], which were confirmed by numerous subsequent investigations. These researchers observed that the growth rates of small cracks were higher than those of long cracks when correlated using the stress intensity factor range.

The typical crack growth rates of small and long cracks are schematically shown in Fig. 2.2. For long cracks, the growth rate generally increases with increasing ΔK. There is also a threshold stress intensity factor range (ΔK_{th}) below which the crack growth rate is so small (less than 10^{-10} m/cycle) that the crack is regarded to be dormant. Small cracks can exhibit a variety of behaviors that are generally influenced by the microstructure. They can grow when subjected to nominal ΔK values below ΔK_{th}. It is also seen that different small crack growth rates occur at the same ΔK value. Small cracks may arrest or slow down due to the interaction with microstructural barriers. A small crack may also continue to grow until its growth rate merges with that of long cracks.

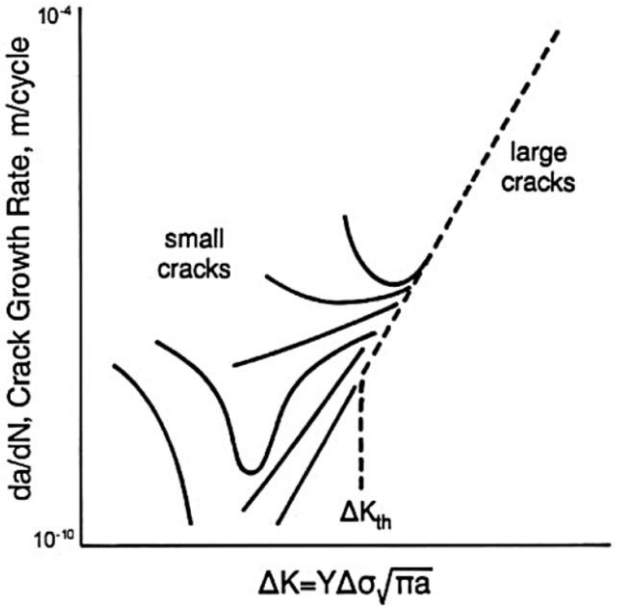

Figure 2.2 - Typical variations of crack growth rate with stress intensity factor range for small and long cacks, for constant amplitude loading (modified from [20,29]).

To further show the inadequacy of LEFM parameters to predict small crack growth rate, the test data produced by Nisitani and Goto [19] is reproduced in Fig. 2.3. The tests were conducted on plain specimens made of 0.45% carbon steel, which were subjected to fully reversed axial loading at four stress ranges (640, 580, 510, and 460 MPa). The crack growth

rates were measured for surface crack lengths from 0.05 to 1.5 mm. The data in Fig. 2.3 clearly show that small crack growth rate cannot be uniquely determined by the stress intensity factor range, ΔK, used for long cracks. This limitation occurs because the condition of small-scale yielding is not satisfied, in general, when the crack length is small.

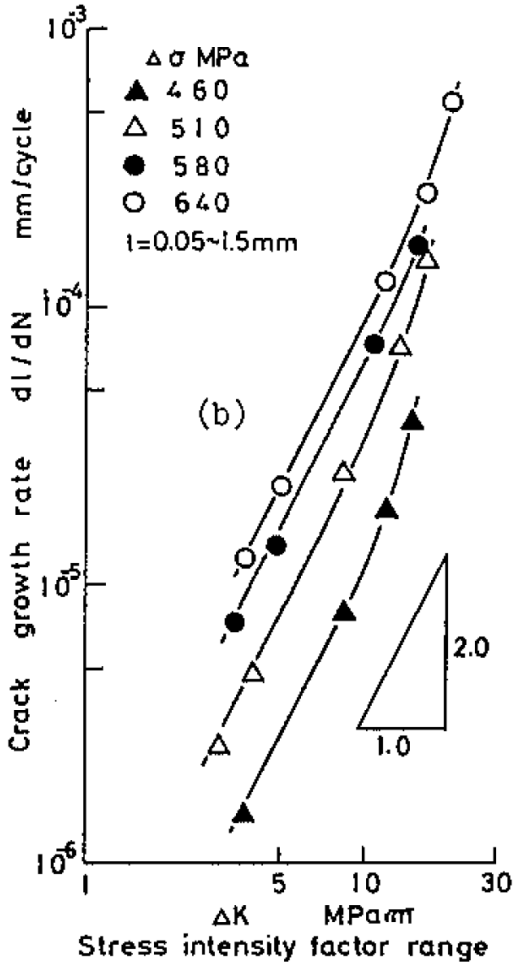

Figure 2.3 - Small crack growth rate in a 0.45% C steel plain specimen subjected to fully reversed axial loading (modified from [19]).

The small crack growth data shown in Fig. 2.3 is for medium carbon steel without a small defect. As the present study concerns the propagation of small cracks from a small defect, it is worthwhile to present some test data that demonstrate the limitation of LEFM in such situations. Fig. 2.4 shows the small fatigue crack growth rates in cast A356-T6 aluminum alloy reported

in Ref. [30]. The cracks were initiated from artificial micro notches, of approximately 200 μm in length, which were used to simulate the surface porosities where cracks are usually formed in cast aluminum. A look at Fig. 2.4 confirms the inadequacy of the ΔK parameter in reducing small crack growth rates to a single curve.

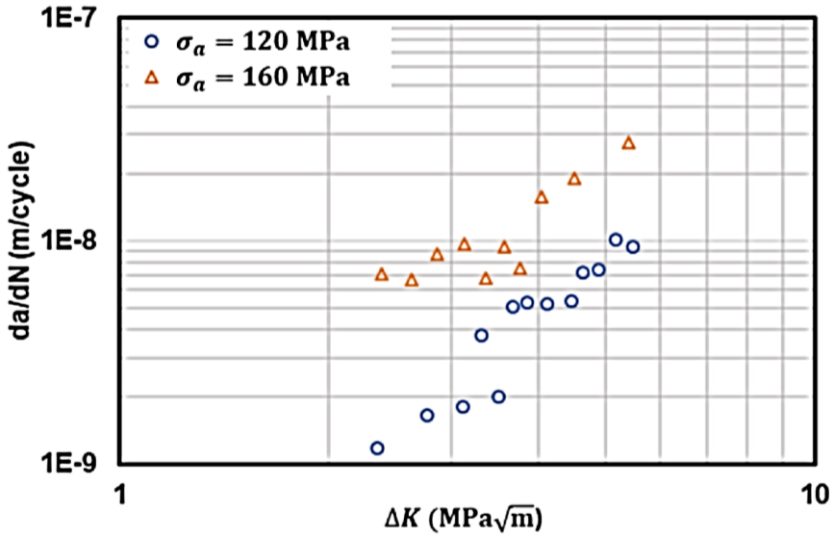

Figure 2.4 - Small crack growth rate for cast A356-T6 aluminum alloy subjected to fully reversed axial loading (reproduced from [30]).

Another example where LEFM fails to describe small crack growth behavior is shown in Fig. 2.5. The test data were reported in [23] and refer to a 0.42% carbon steel with a drilled hole of diameter and depth equal to 0.3 mm. The tests were conducted under fully reversed axial loading. The results in Fig. 2.5 indicate that for stress amplitudes higher than 230 MPa the crack growth rate at a given ΔK value depends on the stress amplitude (i.e., the crack growth rate cannot be uniquely calculated using ΔK). This limitation of LEFM in describing the data can be attributed to the violation of the small scale yielding condition.

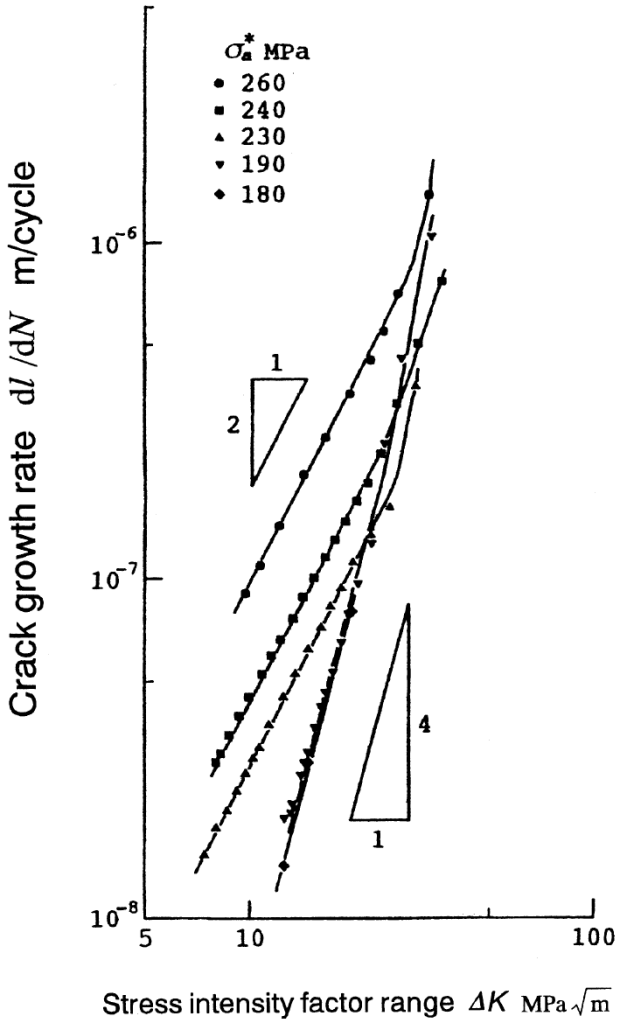

Figure 2.5 - Small crack growth rate for 0.42% carbon steel with a small cylindrical hole, subjected to fully reversed axial loading (reproduced from [23]).

Since LEFM parameters are usually inadequate to handle small fatigue cracks, many studies [9,19,21–25] have tried to identify a mechanical parameter capable of predicting small crack growth. A selection of these parameters is reviewed in the next sections.

2.3. Models for predicting small fatigue crack growth

2.3.1. Nisitani model (1986)

To find an evolution rule for small fatigue crack growth, Nisitani and co-workers performed successive measurements of surface crack length on different metallic materials [19,23,24]. In an earlier study [19], the material investigated was 0.45% carbon steel. The tests were conducted on plain specimens and on specimens containing a drilled hole with a diameter and depth of 0.1 mm, which were subjected to fully reversed tension-compression. Based on the experimental results obtained, it was found that the growth rate of a small crack can be determined by the relation

$$\frac{\mathrm{d}l}{\mathrm{d}N} = B_N \sigma_{\mathrm{a}}^{j} l \tag{2.3}$$

where σ_{a} is the stress amplitude and l is the crack length. The symbols B_N and j represent constants that depend on the material and testing conditions. The reasoning behind relation (2.3) is that the crack growth rate is proportional to the size of the crack tip plastic zone which, in turn, depends on the magnitude of the stress amplitude and the crack length.

The effectiveness of relation (2.3) in correlating small crack growth data can be checked using a plot of $\mathrm{d}l/\mathrm{d}N$ versus $\sigma_{\mathrm{a}}^{j} l$. Fig. 2.6 shows this type of plot for test data of 0.45% C steel [19]. The crack length was measured on the surface of plain specimens and specimens with a small, drilled hole. The very good correlation of the test data was obtained using an exponent $n = 8$. Further investigation by Goto and Nisitani [24] demonstrated that the small crack growth rate given by Eq. (2.3) is valid not only for medium carbon steels but also for low-alloy steels (JIS SCr440, SCM435, and SNCM439).

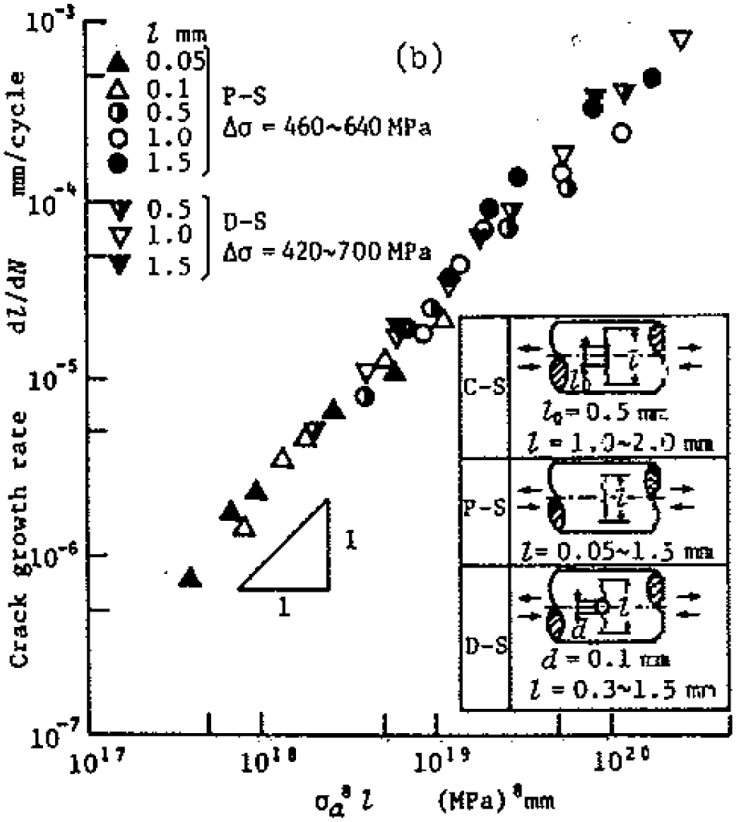

Figure 2.6 - Small fatigue crack growth rate for 0.45% carbon steel (reproduced from [19]).

Nisitani and co-workers [24] also proposed a modification of Eq. (2.3) which is more convenient for comparing small crack growth rates of different materials. The relation is written as

$$\frac{\mathrm{d}l}{\mathrm{d}N} = C_N \left(\frac{\sigma_\mathrm{a}}{\sigma_\mathrm{m}}\right)^k l \tag{2.4}$$

where σ_m is a material property such as the yield stress or the ultimate tensile strength. Empirical expressions for C_N and k as a function of the ultimate tensile strength can be found in [24].

2.3.2. *Model of Caton et al. (2000)*

Later, Caton [25] evaluate a small crack growth relation accuracy on predicting fatigue life of cast 319-type aluminum alloy specimens with two solidification times under fully reversed loadings. His proposed relation is as follows:

$$\frac{\mathrm{d}l}{\mathrm{d}N} = C_C \left[\varepsilon_{\max} \left(\frac{\sigma_\mathrm{a}}{\sigma_\mathrm{y}} \right)^p l \right]^q \tag{2.5}$$

where $\varepsilon_{\max}$ is the remote strain corresponding to the maximum stress level, σ_a is the stress amplitude, σ_y is the monotonic yielding strength, and C_C, p, and q are the material constants. Additionally, Caton adopted the l_i as the pore size and l_f as 3 mm. As the author affirmed, the model is quite insensitive to the definition of l_f [25].

The fatigue life predictions based on small crack growth proved to be the more accurate approach than one based on LEFM. However, it was observed that overestimated predictions for short-life tests on specimens subjected to longer solidification times, which Caton addressed to the multiple crack initiation. Moreover, the model underestimated predictions for long-life tests on specimens subjected to shorter solidification times. The possible reasons are the ineligibility of the assumption that crack nucleate time is negligible or the microstructural barrier effects [25].

2.3.3. *Fatemi model (2021)*

Recently, Fatemi [9] proposed a small crack growth model for multiaxial loadings, based on the maximum principal stress plane. The authors used the Smith–Watson–Topper (SWT) as the fatigue parameter. The model is written as follows

$$\frac{\mathrm{d}l}{\mathrm{d}N} = C_F \left[\left(E \frac{\varepsilon_{1,\mathrm{a}} \sigma_{\mathrm{n,max}}}{\sigma_u^2} \right)^s l \right]^t \tag{2.6}$$

where $\sigma_{n,max}$ and $\varepsilon_{1,a}$ are the maximum normal stress and the amplitude of maximum principal strain on the plane on maximum principal stress, respectively, σ_u is the ultimate tensile strength, and C_F, s, and t are material constants.

The authors performed axial, torsion (fully reversed, mean torsion, and mean compression), in-phase, and out-phase fatigue tests on A356-T6 aluminum alloy. The l_i corresponded to the defect size [9]. The results (Fig. 2.7) indicated that the estimated lives were in good agreement with the experimental data, except for some tests conducted under high stress amplitudes. The author addressed this inaccuracy to the use of cyclic stress-strain relation to calculate strain amplitude. This relation was associated with the strain amplitude in stabilized condition after the hardening process, but in specimens under high stress levels, the hardening process continues until the failure.

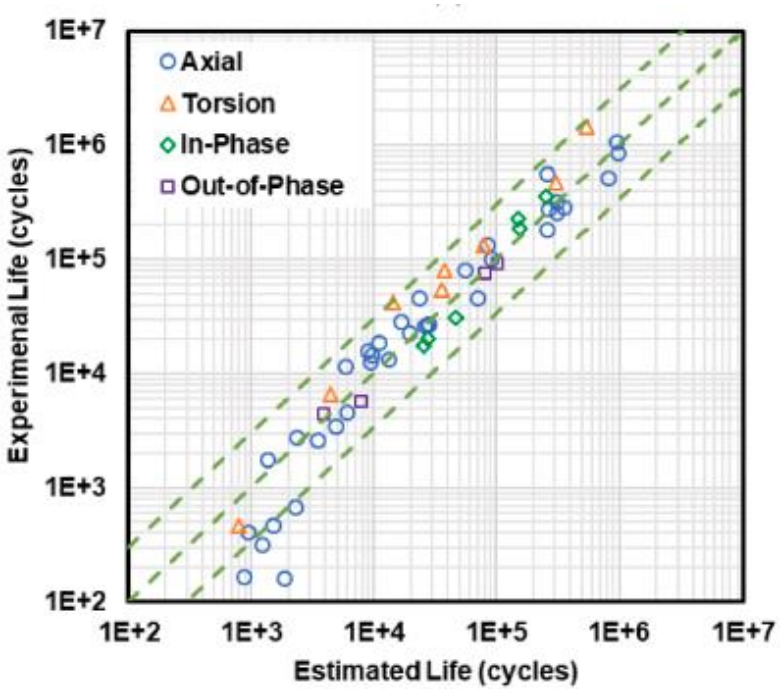

Figure 2.7 - Comparison between experimental fatigue lives of A356-T6 aluminum alloy and estimated lives based on small crack growth (reproduced from [9]).

In a previously work [31], Fatemi verified that the range of plane orientations that experience more than 95% of the maximum fatigue damage is wider for out-of-phase tests than for in-phase tests. In fact, for in-phase tests, the range is 9º, while for out-of-phase, it is 17º. This is the reason for faster crack growth in out-of-phase tests than in in-phase tests. To model it, Fatemi proposed to multiply the Eq. (2.6) by the factor $\sqrt{\theta_{95,OP}/\theta_{95,IP}}$, where $\theta_{95,OP}$ and $\theta_{95,IP}$ are the range of plane orientations experiencing over 95% of the maximum fatigue damage under out-of-phase loading and in-phase loading, respectively [9].

2.3.4. A Walker-type model for small crack growth

As described in the previous section, Fatemi [9] proposed a model for the growth of a crack emanating from a small defect by substituting the uniaxial stress amplitude in the Nisitani [19] relation for the Smith–Watson–Topper parameter [32]. This substitution was done to account for the mean stress effect on fatigue life. Moreover, the model was interpreted in terms of the critical plane approach to make it applicable to defects subjected to multiaxial stress and strain histories.

In this section, the Fatemi small crack growth model will be modified by substituting the Smith–Watson–Topper parameter for one similar to the Walker parameter [33]. This modification was an attempt to improve the life estimates of the Fatemi model for the fatigue tests conducted in the present work involving mean stress (see Chapter 3). The improved life estimates obtained using a Walker-type parameter will be demonstrated in Chapter 4.

The formulation of the new model has a phenomenological character, i.e., it is based on the observation of the process of initiation and growth of a crack at a small defect. A commonly adopted assumption (see, e.g., Ref. [9]) is that the crack initiation period can be neglected since the stress and strain concentration at the edge of the defect will rapidly induce the appearance of a very small crack. A further assumption is that a defect with a crack can be treated as an

equivalent crack whose size is given by the defect size plus the size of the emanating crack (or cracks). This approach is illustrated in Fig. 2.8 for the simple case of a hole under uniaxial stress, where l is the total crack length.

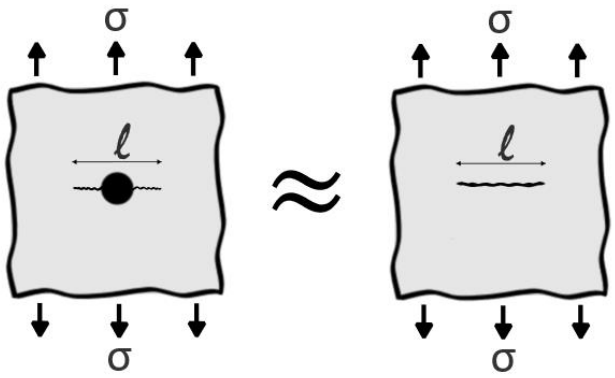

Figure 2.8 – Schematic of a surface with a small hole with cracks and its equivalent crack.

As the crack initiation period is neglected in the present framework, the total fatigue life is assumed to be approximately equal to the sum of a period of small crack growth with a period of long crack growth. For the specimen and loading conditions under investigation here (see Chapter 3), it was observed that the number of loading cycles spent on propagating a long (macroscopic) crack up to the total fracture of the specimen was short relative to the total fatigue life. Therefore, the total fatigue life was considered to be approximately equal to the life spent on small crack growth.

The selection of the driving forces for small crack growth was based on experimental evidence [34–37] that has indicated that medium carbon steel with a small defect fails by tensile crack growth. This observation suggests that the rate of small crack growth from a defect should depend on quantities involving the stress and strain normal to the crack plane. As illustrated in Fig. 2.9, it can be assumed these quantities as the normal strain amplitude $\varepsilon_{\mathrm{na}}$ and the maximum normal stress σ_{nmax}. Moreover, the rate of small crack growth per loading cycle, $\mathrm{d}l/\mathrm{d}N$, is assumed to follow the relation

$$\frac{\mathrm{d}l}{\mathrm{d}N} = C(FP)^m l^n \tag{2.7}$$

where FP denotes the fatigue parameter given by

$$FP = (E\varepsilon_{\mathrm{na}})^{\xi}\sigma_{\mathrm{nmax}}^{1-\xi} \tag{2.8}$$

In the above expressions, the symbols *C*, *m*, *n* and, ξ are constants that have to be found by fitting small fatigue crack growth data. The orientation of the critical plane is defined by the criterion of maximum crack growth rate, which corresponds to the plane where the fatigue parameter expressed by Eq. (2.8) has maximum value. The search for the critical plane follows the standard procedure of the critical plane approach [38]: the fatigue parameter on each plane is calculated with the help of the well-known strain and stress transformation equations of Solid Mechanics, and then the critical plane is identified as the one where the fatigue parameter is maximum.

Note that the parameter (2.8) generalizes the Smith–Watson–Topper parameter by powering the quantities $E\varepsilon_{\mathrm{na}}$ and σ_{nmax} to a fitting constant ξ, instead of powering them to 0.5 as in the original parameter. The idea of using this fitting exponent was introduced by Walker [33] in the context of a stress-based parameter similar to that proposed by Smith, Watson, and Topper. Also, note that the above formulation is a modification of the small crack growth model developed by Fatemi. In fact, for $\xi = 0.5$, when $n = t$, $m = 2st$, and $C = C_{\mathrm{F}}/(\sigma_{\mathrm{y}}^{m}E^{m/2})$ the above formulation turns into the Fatemi model given by Eq. (2.6).

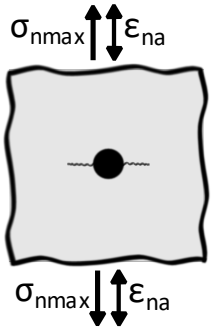

Figure 2.9 – Quantities governing mode I (tensile) crack growth from a small defect: the normal strain amplitude and the maximum normal stress on the critical plane.

To calculate the number of cycles to failure, N_f, the relation (2.7) has to be integrated from an initial crack size l_i (here equal to the defect size) to the size of a macroscopic crack l_f, which typically is around 2–3 mm. Since the fatigue parameter does not depend on the crack size, this integration yields

$$N_\mathrm{f} = \frac{1}{C(FP)^m} \int_{l_\mathrm{i}}^{l_\mathrm{f}} \frac{1}{l^n}\, dl \tag{2.9}$$

whose closed-form solution when $n \neq 1$ has the form

$$N_\mathrm{f} = \frac{1}{C(FP)^m} \frac{l_\mathrm{f}^{1-n} - l_\mathrm{i}^{1-n}}{1-n} \tag{2.10}$$

Moreover, when $n = 1$, which will be shown in Chapter 4 to be the case for the 1045 steel under investigation, the solution is given by

$$N_\mathrm{f} = \frac{1}{C(FP)^m} \ln \frac{l_\mathrm{f}}{l_\mathrm{i}} \tag{2.11}$$

3. MATERIAL AND METHODS

The material investigated in this study is the SAE 1045 carbon steel. Its chemical composition in weight percentage is 0.46 C, 0.66 Mn, 0.19 Si, 0.012 S, 0.022 P, and Fe as balanced, as informed by the provider. The material was acquired in the form of cylindrical bars with a diameter of 19.05 mm. To relieve the residual stresses due to the manufacturing process, the bars were annealed at 850 ºC for 45 minutes.

The material mechanical properties were taken from [10], a work that evaluated specimens originating from the same batch and subjected to the same heat treatment. The referenced work performed a tensile test to evaluate the monotonic properties, which resulted in the stress-strain curve shown in Fig. 3.1. The mechanical properties values found by the authors are listed in Table 1. Additionally, in the mentioned study, the Vickers hardness estimation was 199 kgf/mm^2. However, in the present work, the Vickers hardness was also estimated, following the ASTM E92 recommendations [39]. It was made four measurements on the edge of a specimen transversal section by applying 30 kgf. The authors defined the Vickers hardness as the arithmetic media between the measurements and obtained 189 kgf/mm^2. The value is consistent with [10] and was considered during this work.

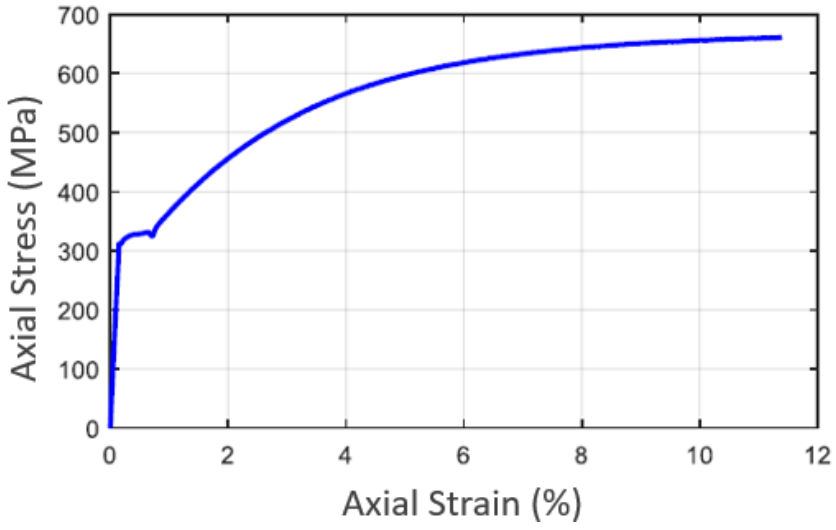

Figure 3.1 – Stress-strain curve of 1045 steel under tensile loading (reproduced from [10]).

Table 1 - Mechanical properties of the SAE 1045 carbon steel.

Young's modulus	216 GPa
0.2%-offset yield stress	326 MPa
Ultimate tensile strength	661 MPa
Reduction in area	31%
Vickers hardness	189 kgf/mm²

Data reproduced from [10].

To examine the microstructure of the material, the specimen was cut in a transversal and longitudinal direction to its axis. Then, a chemical etching process was applied to surfaces using a solution of Nital 10%. Subsequently, the treated surfaces were subjected to analysis employing an Olympus LEXT OLS4100 3D confocal laser microscope. The resulting micrographs of the transversal and longitudinal surfaces to the specimen axis are shown in Fig. 3.2. Given that this material is classified as hypoeutectoid steel and it was subjected to annealing, it is expected that a microscopic evaluation of its structure reveals the presence of proeutectoid ferrite and perlite microconstituents which indeed was observed. Additionally, the average grain size determined using the Intercepted Method [40], yielded an estimated value of 15 μm. It was not verified a significant difference between the transversal and longitudinal surfaces grain size.

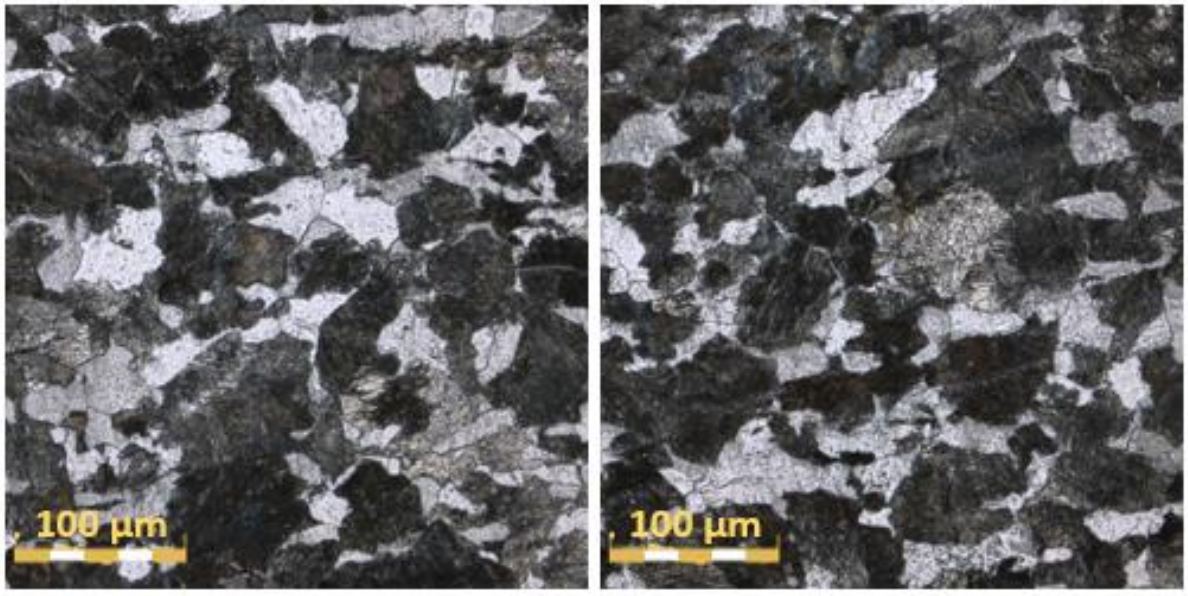

Figure 3.2 - Micrograph of the 1045 steel etching transversal (a) and longitudinal (b) surface to the specimen axis with Nital 10%.

Cylindrical solid specimens as shown in Fig. 3.3 were machined according to the ASTM standard E466 [41]. The surface of each specimen was ground in the gage section using sandpapers with grit numbers ranging from 220 to 2500. The surface roughness was measured using an Olympus LEXT OLS4100 3D confocal laser microscope and complied with the ASTM standard E466 specifications [41], which recommends that the Ra parameter must be less than 0.1 µm. After grinding, a cylindrical blind hole with a diameter and depth of 400 µm was milled in the middle of the gage section of the specimen, with a Vega Model MVU 920 Vertical Machining Center. A micrograph of the artificial hole before testing is shown in Fig. 3.4.

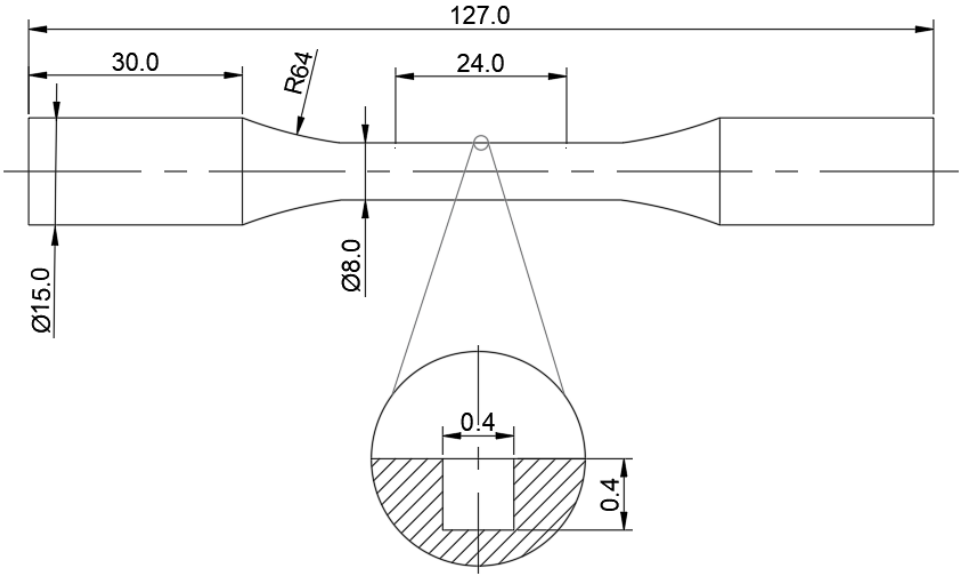

Figure 3.3 - Specimen used in the fatigue tests (dimensions in mm).

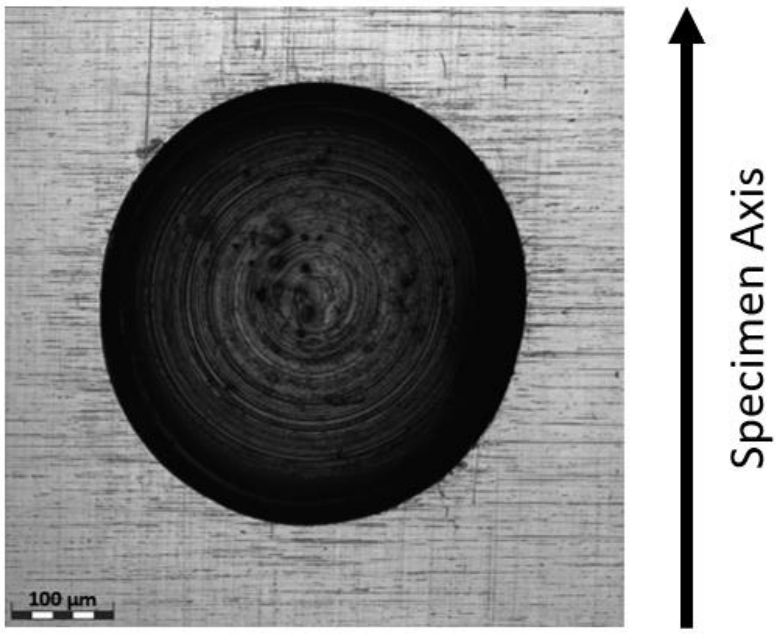

Figure 3.4 - Micrograph of the artificial blind hole milled into the specimen surface.

3.1. Fatigue tests

The fatigue tests were performed under force control using an MTS servo-hydraulic machine with a capacity of 100 kN in axial force. The specimens were subject to sinusoidal uniaxial loading at load ratios R of -1 and 0.1. The tests were carried out until the complete fracture of the specimen or were interrupted at the run-out condition (10^7 cycles). Table 2 lists the loading conditions and the corresponding number of cycles to failure. It should be noted that some of the test data were previously produced by [10] using the same 1045 steel. Furthermore, S-N curves of 1045 steel with a blind hole with a diameter and depth of 400 μm at load ratios R = -1 and R = 0.1 are shown in Fig. 3.5.

Table 2 - Fatigue test data of 1045 steel with a cylindrical blind hole with a diameter and depth of 400 μm.

Loading Type	$\boldsymbol{\sigma_{xa}}$ (MPa)	$\boldsymbol{\sigma_{xm}}$ (MPa)	$\boldsymbol{N_f}$ (cycle)	Source
Axial, $R = -1$	250	0	28,317	
	220	0	87,000	[10]
	220	0	90,028	
	208.5	0	341,099	
	208.5	0	372,457	
	200	0	450,000	[10]
	185	0	1,575,000	
	185	0	3,000,980	
	180	0	5,700,000	[10]
	160	0	$>10^7$	[10]
	185	0	3,000,980	
Axial, $R = 0.1$	167.7	205.2	207,189	
	165	201.7	288,326	
	165	201.7	344,992	
	150	183	670,000	[10]
	150	183	546,805	
	147	180.1	547,325	
	140	171.1	1,606,463	
	130	159	$>10^7$	[10]

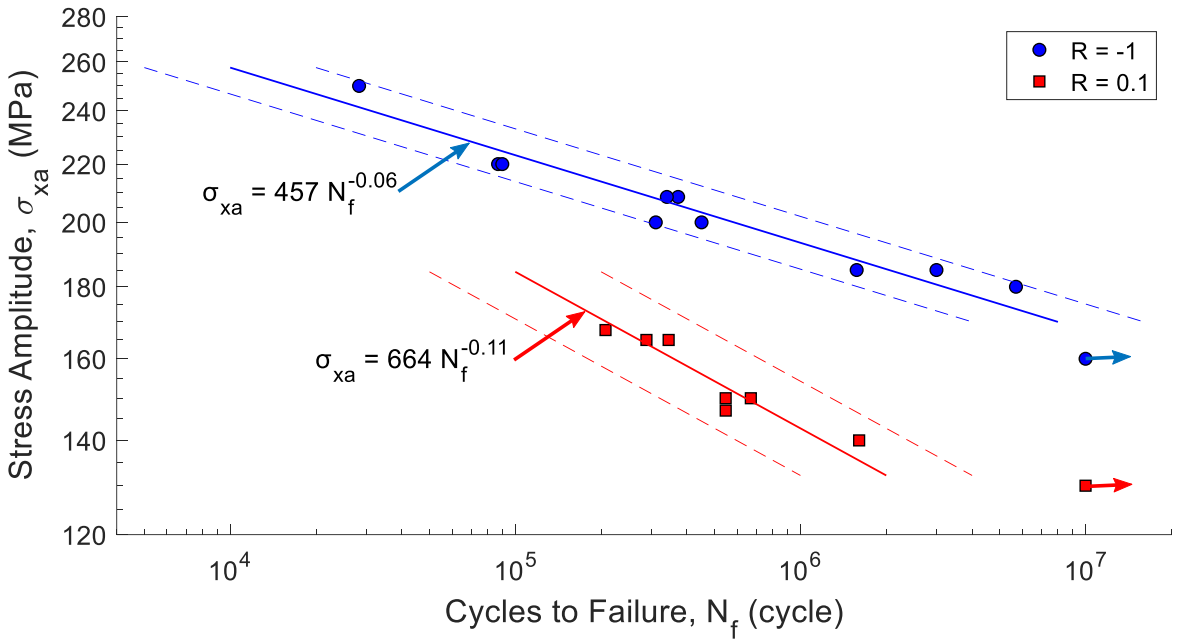

Figure 3.5 - S-N data of 1045 steel with a cylindrical hole with a diameter and depth of 400 µm.

3.2. Measurement of small crack growth rate

The evolution of crack length during a fatigue test was determined by periodically interrupting the test, taking the specimen to a confocal laser microscope, and measuring the crack length. The equipment enabled the identification of an increase of, approximately, 10 µm in crack length, which is smaller than the average grain size. The crack length evolution was monitored until it reached, approximately, 1.5 mm, which is the maximum length that could be precisely measured using the confocal laser. To enhance visibility and allow more accurate measurements, the cracks formed at the left and right sides of the microhole were examined separately. Figures 3.6 and 3.7 present a sequence of images that shows the crack evolution during the test conducted at $R = 0.1$ ($\sigma_{xa} = 165$ MPa, $\sigma_{xm} = 201.7$ MPa, and $N_f = 344{,}992$ cycles).

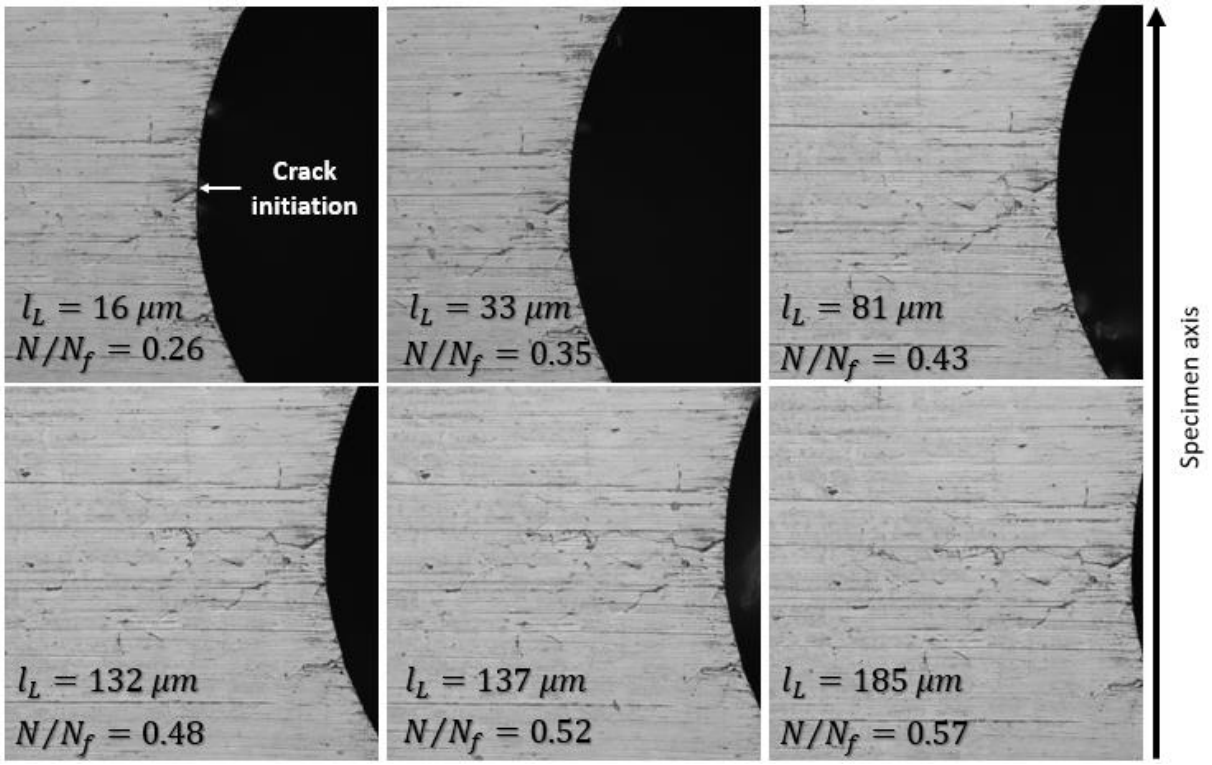

Figure 3.6 – Crack growth at the left side of the microhole during a test conducted at R = 0.1 (σ_{xa} = 165 MPa, σ_{xm} = 201.7 MPa, and N_f = 344,992 cycles).

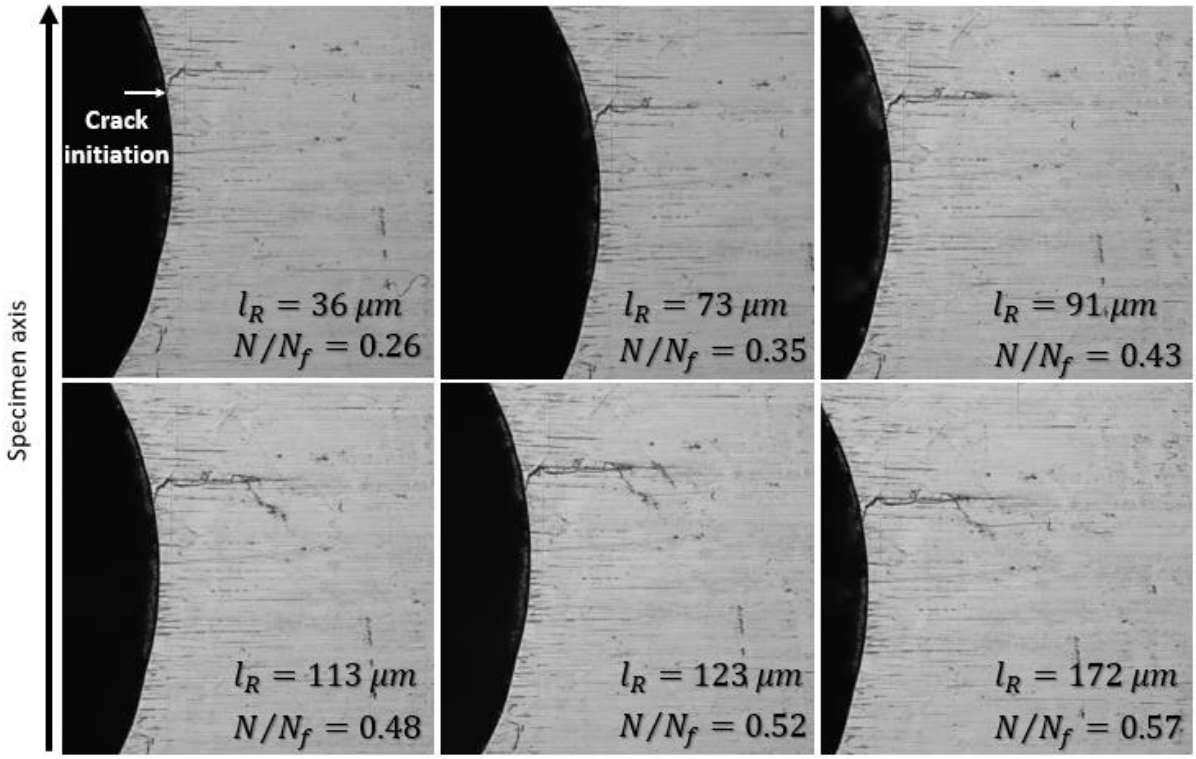

Figure 3.7 - Crack growth at the right side of the microhole during a test conducted at R = 0.1 (σ_{xa} = 165 MPa, σ_{xm} = 201.7 MPa, and N_f = 344,992 cycles).

The total crack length, l, was defined as the sum of the hole diameter, the left crack length, and the right crack length, as illustrated in Fig. 3.8. For instance, Fig. 3.9 shows micrographs of the fatigue cracks emanated from the hole of the specimen tested at σ_{xa} = 250 MPa and R = -1. These images were taken at 9,500 loading cycles. The crack length was 632 µm, which was the sum of the hole diameter of 400 µm, the left crack length of 59 µm, and the right crack length of 173 µm.

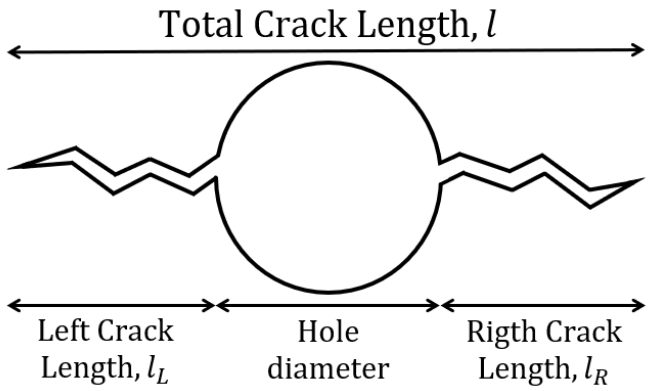

Figure 3.8 - Scheme for the definition of crack length.

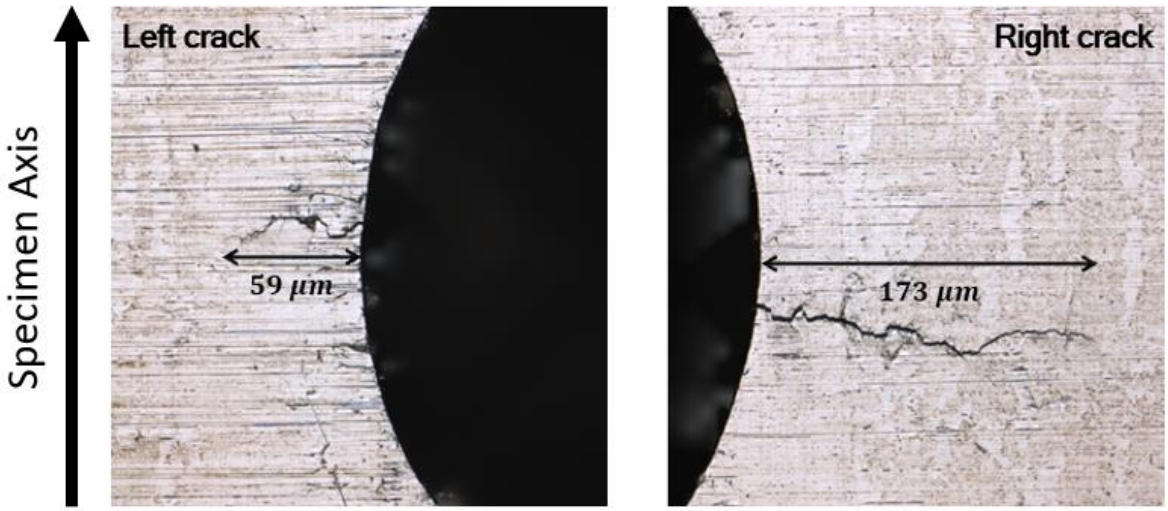

Figure 3.9 - Fatigue cracks at the hole of a specimen tested at σ_{xa} = 250 MPa and R = -1. Images taken at 9,500 loading cycles.

The crack growth rate, dl/dN, was calculated using the incremental polynomial method described in ASTM Standard E647-15 [42]. This algorithm entails fitting a second-order polynomial (parabola) to 2n+1 successive points. As demonstrated in Fig. 3.10, crack growth rate when $l = l_i$ is defined as the parabola derivative on $\hat{l}_i$, which corresponds to the crack length when $N = N_i$ according to the fitting curve. The fitted value of crack length and crack growth rate are, as follows:

$$\hat{l}_i = b_0 + b_1\left(\frac{N_i - C_1}{C_2}\right) + b_2\left(\frac{N_i - C_1}{C_2}\right)^2 \tag{3.1}$$

$$\left.\frac{\mathrm{d}l_i}{\mathrm{d}N}\right|_{\hat{l}_i} = \frac{b_1}{C_2} + \frac{2b_2(N_i - C_1)}{C_2^2} \tag{3.2}$$

where N_i is the number of cycles, b_0 b_1 and b_2 are regression parameters determined by the least square method and C_1 and C_2 are used to scale the input data. For this research, the value of n is set to 2. The method was implemented in MATLAB. The code was validated based on an output example from the Incremental Polynomial Method Computer Program available in Appendix X1 of ASTM Standard E647-15 [42].

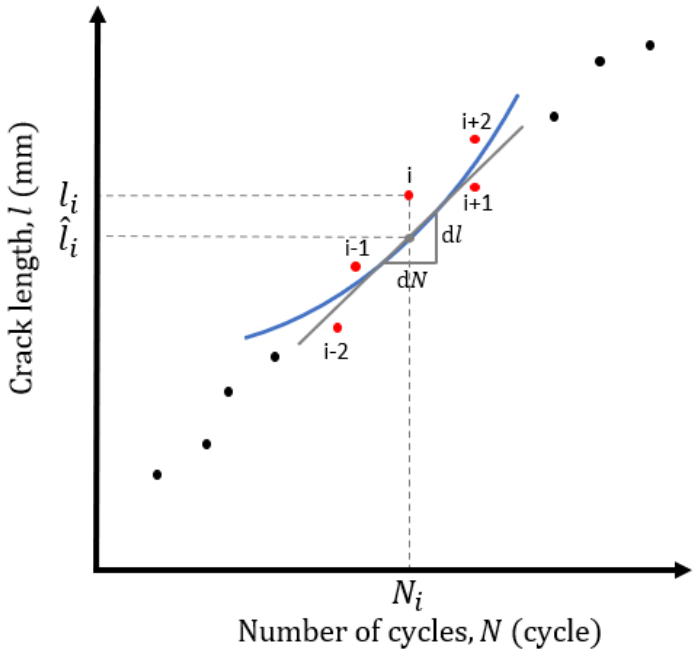

Figure 3.10 – Definition of crack growth rate, dl/dN, according to the incremental polynomial method.

4. RESULTS AND DISCUSSION

4.1. Influence of small crack growth on fatigue life

Figures 4.1a and 4.1b show the correlation between crack length and fatigue life fraction N/N_f in tests conducted at stress ratios of -1 and 0.1, respectively. The test data indicate that a visible crack of approximately 10 µm was detected at $N/N_f = 0.2$. Additionally, it was observed that 70% of the total fatigue life was consumed during the crack growth up to a length of 1.5 mm. Therefore, a significant portion of the total fatigue life, approximately 50%, was spent on small crack growth.

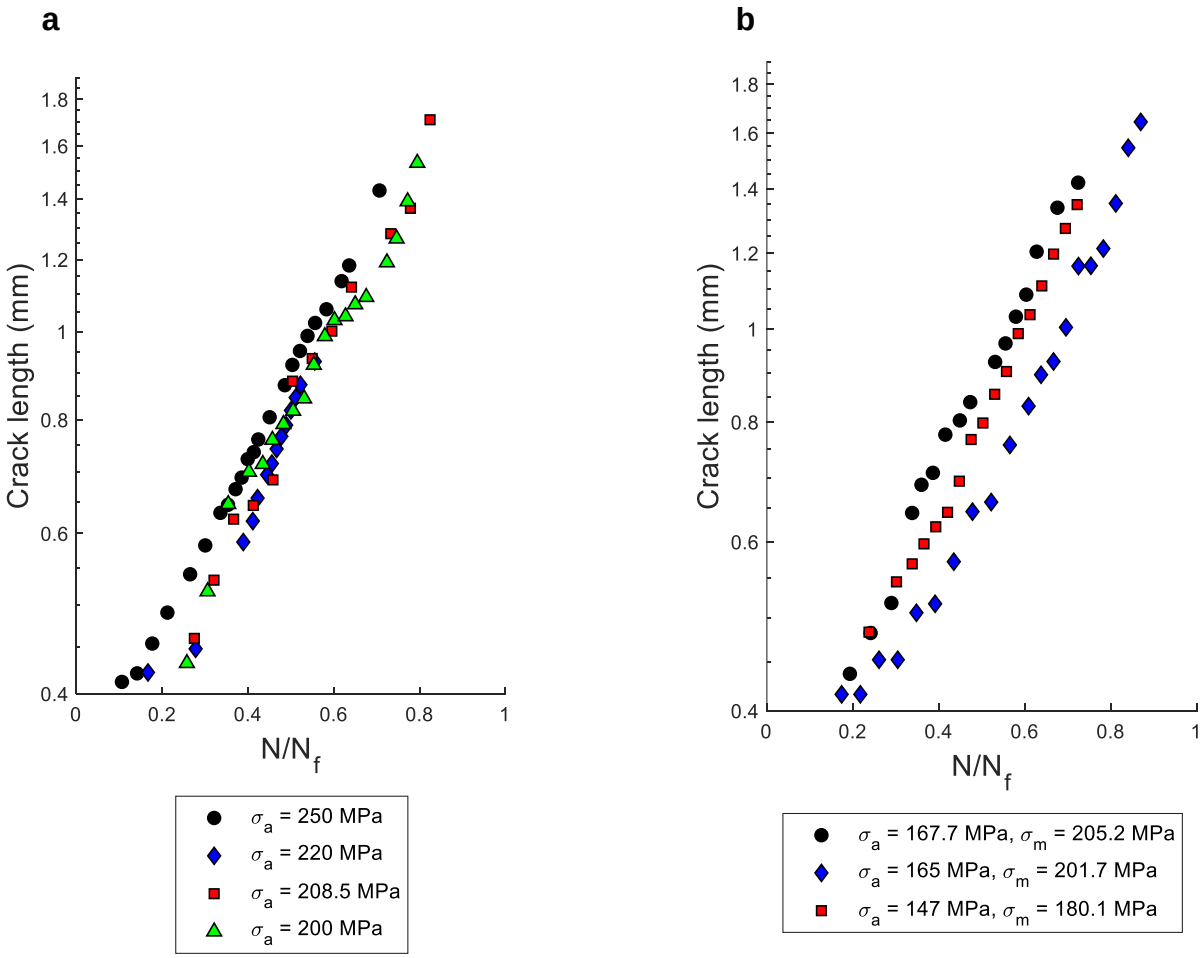

Figure 4.1 - Correlation between crack length and fatigue life fraction for tests conducted under stress ratios of -1 (a) and 0.1 (b).

As mentioned in Chapter 2, when a specimen contains a small defect, a significant portion of its fatigue life is spent on the small crack growth phase. However, the definition of the small crack growth phase is only qualitative. The diagrams presented above illustrate that 20% of the fatigue life is consumed for a crack to reach 10 μm, and an additional 30% is spent for a crack to grow from 1.5 mm to the critical size. Therefore, the assumption that the small crack growth phase concludes at 1.5 mm may lead to overly conservative predictions. An approach aimed to provide better predictions involves considering that this phase extends until the crack propagates up to 2-3 mm. This will be discussed in more detail in a following section.

4.2. Determination of material constants

Figures 4.2a and 4.2b show the correlation between crack growth rate and crack length for the tests conducted under stress ratios R of -1 and 0.1, respectively. The slope of the line corresponds to the constant n in the model given by relation (2.7), which is approximately 1 for all tests. The data suggests that this relation describes more effectively the experimental data for higher stress amplitude tests, where the crack growth rate follows a linear trend in the log-log diagram without significant fluctuations. However, for lower amplitude tests, substantial dispersions are observed. This behavior is expected, since the microstructure barriers, like grain boundaries, act more intensively in these cases.

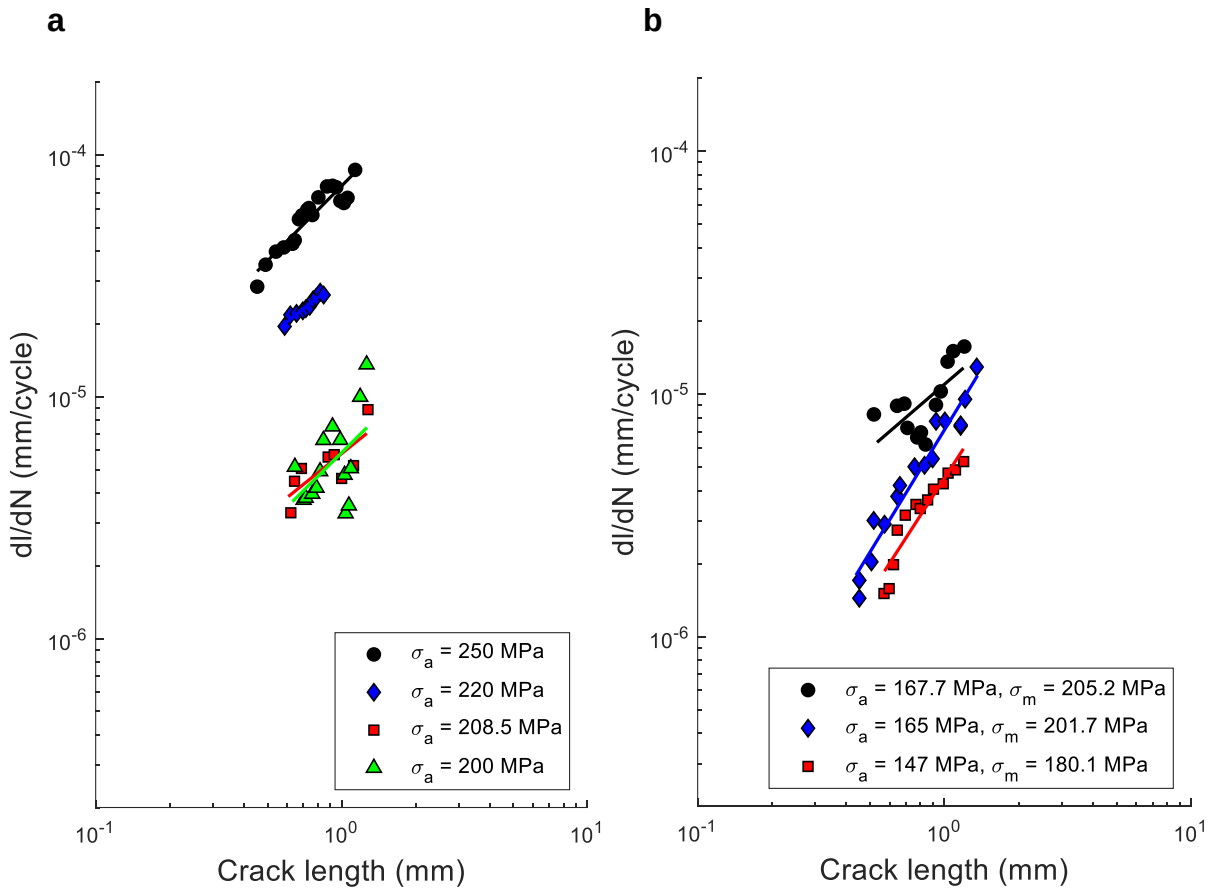

Figure 4.2 - Crack growth rate vs. crack length for the fatigue tests under stress ratios of -1 (a) and 0.1 (b).

To determine the constants *C*, *m*, and ξ, it was plotted d*l*/d*N* versus the term $(FP)^m l^n$ on a log-log diagram. The fully reversed data were used to estimate *C* and *m* values, which resulted in $C = 1.68\times10^{-32}$ and $m = 11.5$ (Fig. 4.3). The constant ξ was determined by finding the value that resulted in the best fit between the small crack growth model and the test data under a stress ratio of 0.1. The best fit was achieved for $\xi = 0.7$ (Fig 4.4a). Also, when $\xi = 0.5$ the fatigue parameter corresponds to Smith–Watson–Topper, which was proposed as the crack driving force by Fatemi. However, as shown in Fig. 4.4b, it did not correlate well with the experimental data.

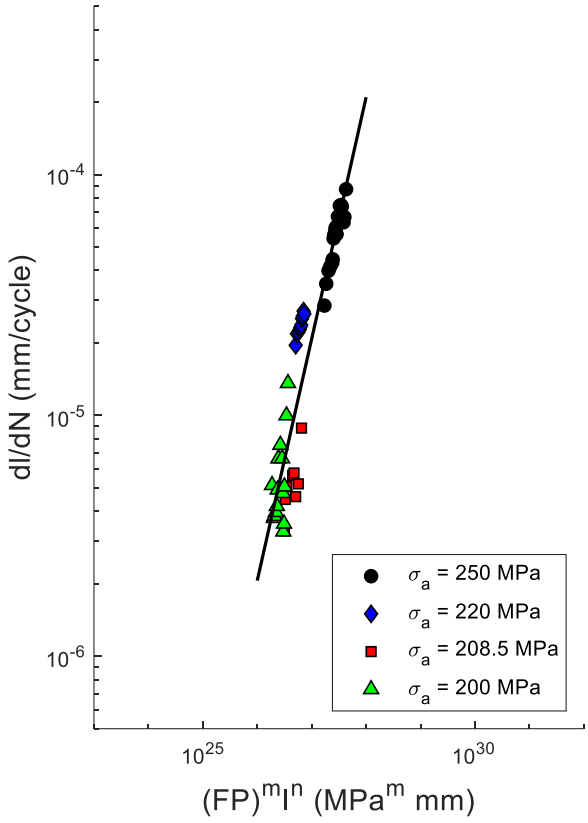

Figure 4.3 - Crack growth rate (d*l*/d*N*) versus the term $(FP)^m l^n$ for fully reversed tests.

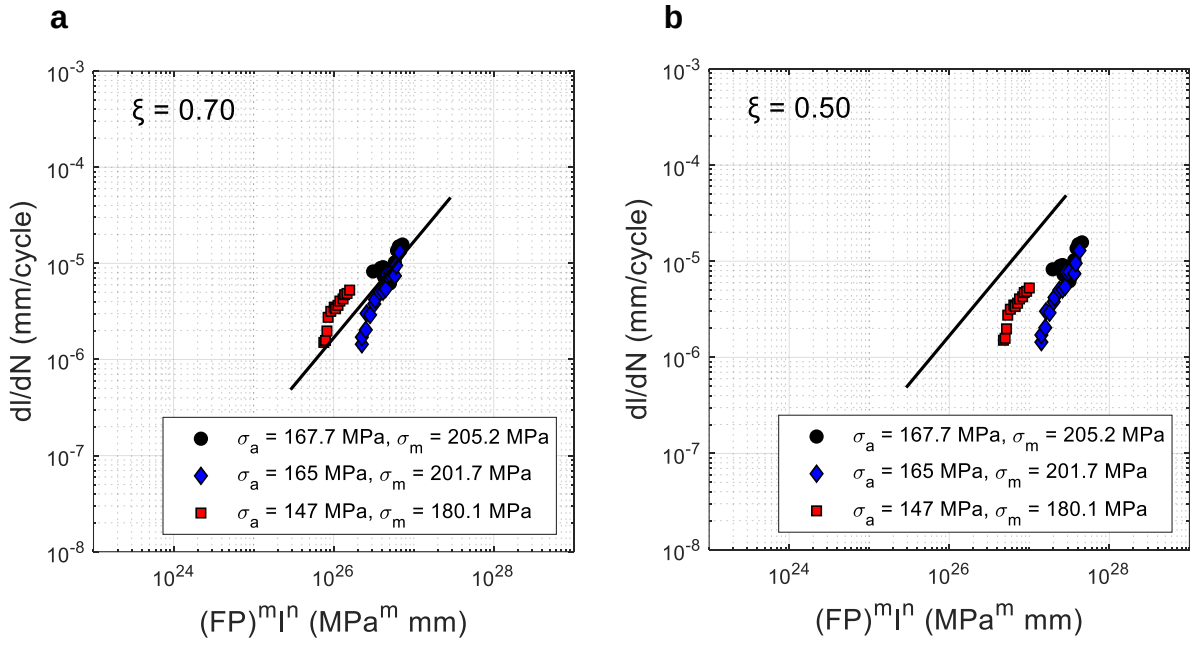

Figure 4.4 - Crack growth rate (d*l*/d*N*) versus the term $(FP)^m l^n$ for tests conducted under a stress ratio of 0.1 when $\xi = 0.7$ (a), $\xi = 0.5$ (b).

4.3. Evaluation of fatigue life prediction

In this section, it is discussed the fatigue life estimation for a 1045 steel containing a small defect subjected to various stress trajectories (axial, torsional, axial/torsional in-phase, and out-of-phase) based on a small crack growth model. Here, a proposed enhancement of the Fatemi model for small crack growth will be evaluated. The improvement attempt consists of substituting the Smith–Watson–Topper parameter for a Walker-type parameter, as detailed previously.

As stated, the form of the small crack growth model assessed in this work is given by Eq. (2.7). To predict the number of cycles to failure, this Equation has to be integrated from an initial crack length, l_i, to a final crack length, l_f. As demonstrated in the section dedicated to the determination of material constants, $n = 1$. Therefore, the integration of Eq. (2.7) yields:

$$N_{\mathrm{f}} = \frac{1}{C(FP)^m} \ln \frac{l_f}{l_i} \tag{4.1}$$

in which the fatigue parameter (FP) is given by

$$FP = (E\varepsilon_{\mathrm{na}})^{\xi} \sigma_{\mathrm{nmax}}^{1-\xi} \tag{4.2}$$

The calibration process resulted in the following constant values: $C = 1.68\times10^{-32}$, $m = 11.5$, $n = 1$, and $\xi = 0.7$. It is worth noting that when $\xi = 0.5$ the fatigue parameter corresponds to the Smith–Watson–Topper parameter. In addition, based on the assumption that a defect with a crack can be treated as an *equivalent crack*, this work defined the initial crack length, l_i, as the defect size. Since the analyses were restricted to the evolution of the surface crack, the defect size corresponded to the diameter of the hole, which was 0.4 mm. The final crack length, l_f, was defined as 1.5 mm, which was the maximum crack size that could be accurately measured using the confocal laser microscope.

4.3.1. Evaluation of the fatigue parameter definition on life prediction

Figures 4.5 and 4.6 show the correlation between the model predictions using Smith–Watson–Topper and Walker-type fatigue parameters and the experimental data, within a factor of 3. The results indicated that the model based on the Walker-type parameter performs better, especially for uniaxial and axial/torsional tests in-phase conducted with the presence of mean stress. Additionally, for long-life tests, there are significant dispersions between the fatigue life predictions and the experimental outcomes. Tests conducted under lower stress amplitude levels are more affected by microstructural barriers, leading to hard-to-predict phenomena such as crack growth slow down or crack arrest. Consequently, the model tends to be conservative for these cases.

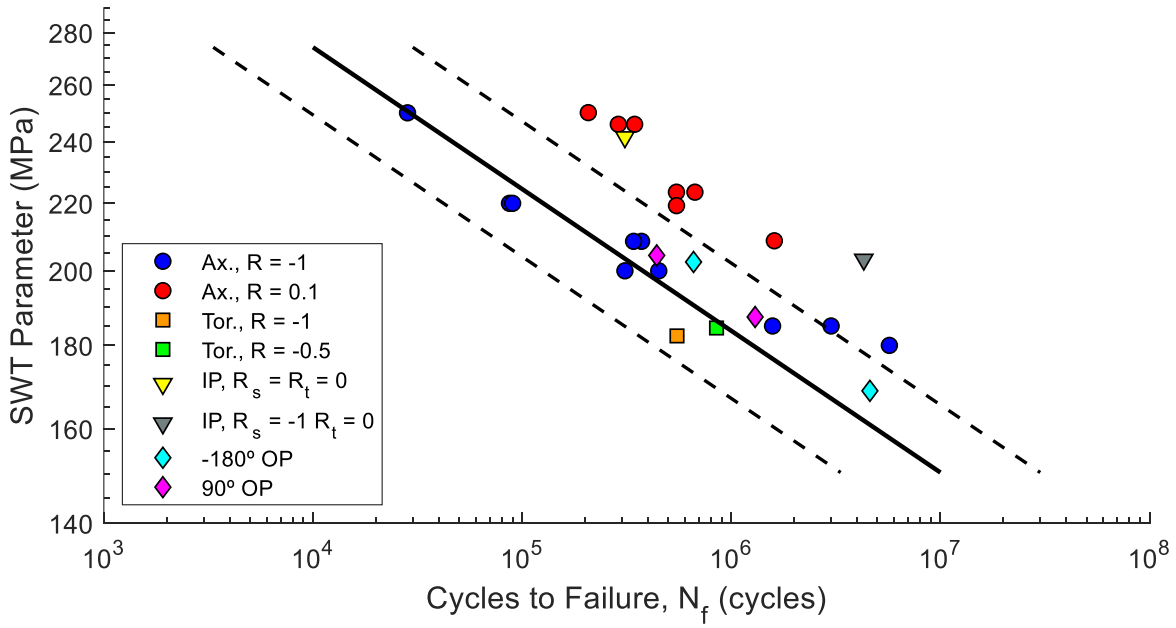

Figure 4.5 - Correlation between the SWT-based model prediction and fatigue life experimental data.

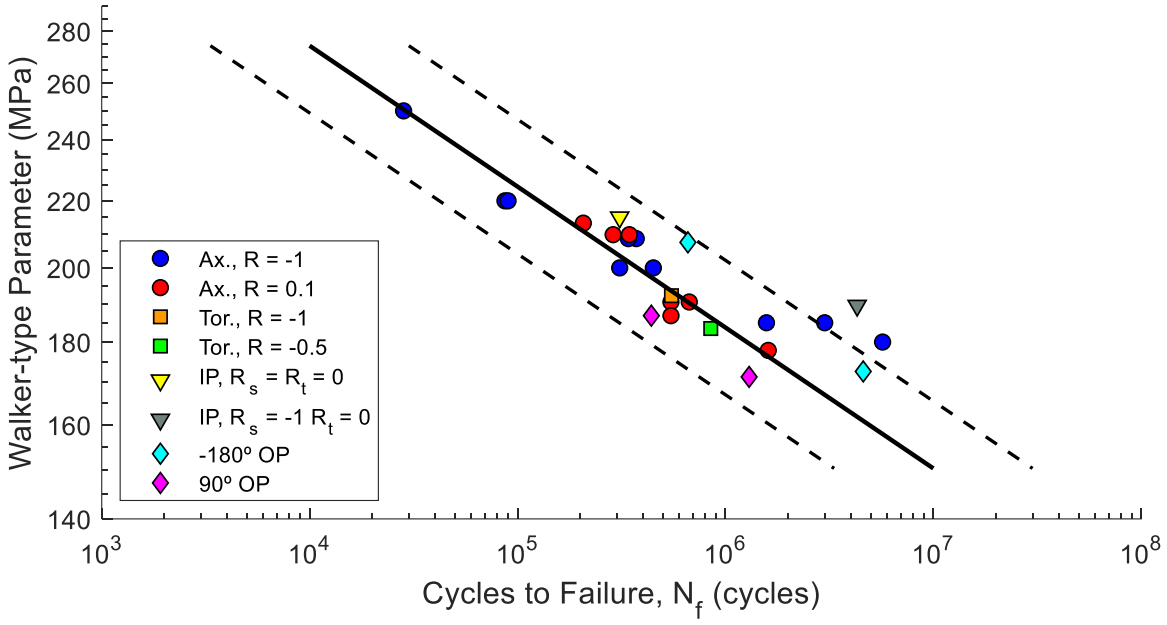

Figure 4.6 - Correlation between the Walker-type-based model prediction and fatigue life experimental data.

4.3.2. Sensibility of the model to final crack length definition

Figures 4.1a and 4.1b show that it required approximately 30% of the fatigue life to a crack propagating from 1.5 mm up to the critical size. Therefore, defining the final crack length, l_f, as 1.5 mm neglects a significant portion of life. This indicates that considering that the small crack growth stage concludes when the crack achieves this length is not reasonable. Hence, the final crack length was increased to 2.5 mm. To assess the sensibility of the model to different final crack length definitions, the estimated fatigue life was compared to the experimental fatigue life for l_f values of 1.5 mm and 2.5 mm. Additionally, the final crack length impact on fatigue life prediction was evaluated for the model based on the SWT parameter and the one based on the Walker-type parameter, as presented in Fig. 4.7a, 4.7b, 4.7c, and 4.7d.

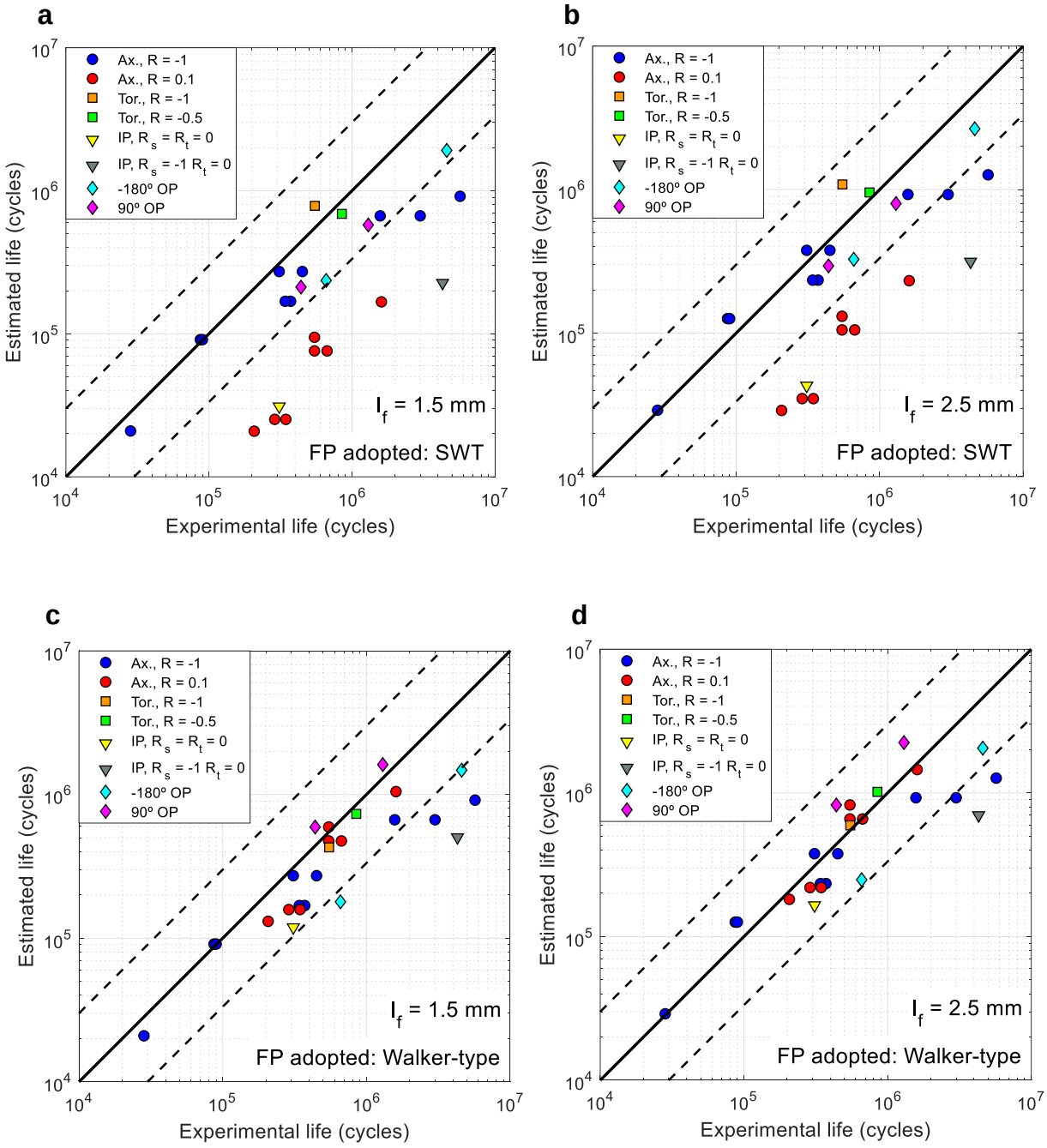

Figure 4.7 - Life prediction based on small crack growth model when adopting: SWT as fatigue parameter and l_f = 1.5 mm (a), SWT as fatigue parameter and l_f = 2.5 mm (b), Walker-type as fatigue parameter and l_f = 1.5 mm (c), and Walker-type as fatigue parameter and l_f = 2.5 mm (d).

A look at Fig. 4.7a and 4.7b states that the model is conservative when using SWT as the parameter, especially for tests that involve mean stress. The Walker-type-based model provides more precise predictions. However, although when l_f = 1.5 mm the estimations are within a factor of 3, a conservatism is still observable, as shown in Fig. 4.7c. This is an expected finding since the model neglects the number of cycles that the crack is classified as a microstructurally small crack and as a long crack.

As shown in Fig. 4.7d, more accurate results were obtained when adopting the Walker-type parameter, and the final crack length is defined as 2.5 mm. However, it is observable that a substantial increase in the l_f (1 mm) did not have a significant impact on the prediction results. The analytical solution provided by Eq. (4.1) reveals that this increase in l_f implies an increment of 39% in fatigue life prediction. Additionally, as the l_f increases, the effect of variations in final crack length on fatigue life estimation decreases. For example, if the final crack length were to be increased by another 1 mm (resulting in a length of 3.5 mm) the additional increment in fatigue life prediction would be 25%.

Ultimately, it is important to highlight that, despite the increase in l_f, the model remained conservative for some tests longer than 2×10^6 cycles. This indicates that the microstructure significantly impacts small fatigue crack growth, especially during tests carried out under lower stress amplitudes.

4.3.3. Analysis of the critical plane criterion

The model proposed here was interpreted using the critical plane approach. To formulate the critical plane criterion, consider a material volume containing a small defect within an x–y–z coordinate system located at the free surface, in which x is parallel to the specimen axis (Fig. 4.8a). A new x'–y'–z' coordinate system can be obtained from the original one by rotating the coordinate axes through an angle θ about the z axis, as shown in 4.8b. The Walker-type Fatigue Parameter on each θ-oriented plane is calculated, and then the critical plane is identified

as the one in which the FP is maximum. Examples of critical plane measurements are shown in Fig. 4.9 and 4.10.

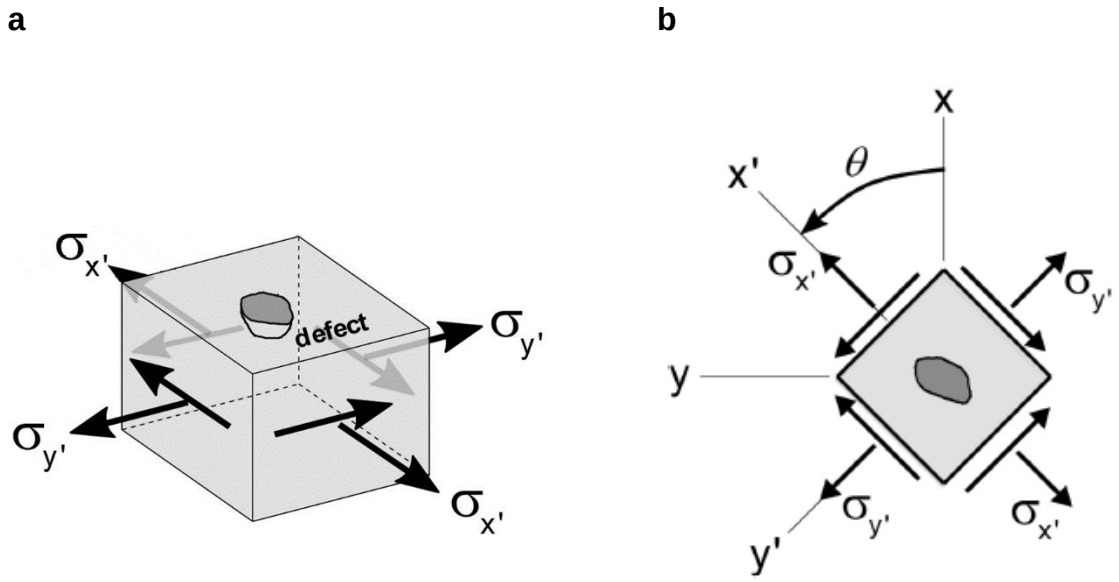

Figure 4.8 – Material volume with a small defect (a) and definition of θ-oriented x'-y'-z' coordinate system (b) (modified from [43]).

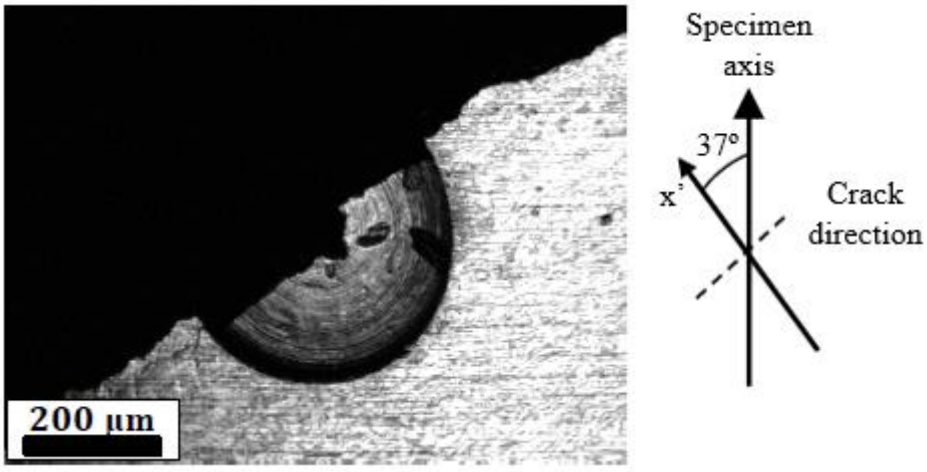

Figure 4.9 - Crack observed from the test under $\sigma_{xa} = \sigma_{xm} = \tau_{xa} = \tau_{xm} = 100$ MPa (axial/torsional in-phase loading path) (modified from [10]).

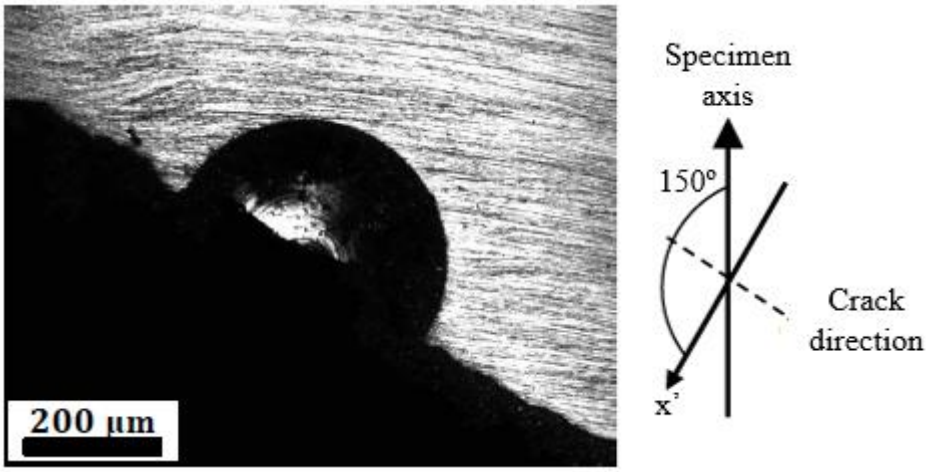

Figure 4.10 - Crack observed from the test under σ_{xa} = τ_{xa} = 120 MPa and σ_{xm} = τ_{xm} = 50 MPa (axial/torsional out-of-phase loading path) (modified from [10]).

Table 3 presents the measured critical planes for torsional and axial/torsional loadings. Fig. 4.11 shows the correlation between the measured critical plane and the estimated critical plane. The predictions are in good agreement with the experimental data.

Table 3 - Measured critical plane for torsional and axial/torsional tests with 1045 steel with a small artificial hole.

ID	Loading	σ_{xa} (MPa)	σ_{xm} (MPa)	τ_{xa} (MPa)	τ_{xm} (MPa)	θ_c (°)	N_f (cycles)
1	Torsion, $R = -1$	160	0	0	0	50	$5{,}5\times10^5$
2	Torsion, $R = 0.5$	140	47	0	0	39	$8{,}5\times10^5$
3	In-Phase, $R_\sigma = R_\tau = 0$	100	100	100	100	37	$3{,}1\times10^5$
4	-180° out-of-phase	120	50	120	50	149	$6{,}6\times10^5$
5	-180° out-of-phase	100	50	100	50	148	$4{,}6\times10^6$
6	In- Phase, $R_\sigma = -1$, $R_\tau = 0$	95	0	95	95	33	$4{,}3\times10^6$
7	90° out-of-phase	120	0	120	120	43	$4{,}4\times10^5$
8	90° out-of-phase	110	0	110	110	41	$1{,}3\times10^6$

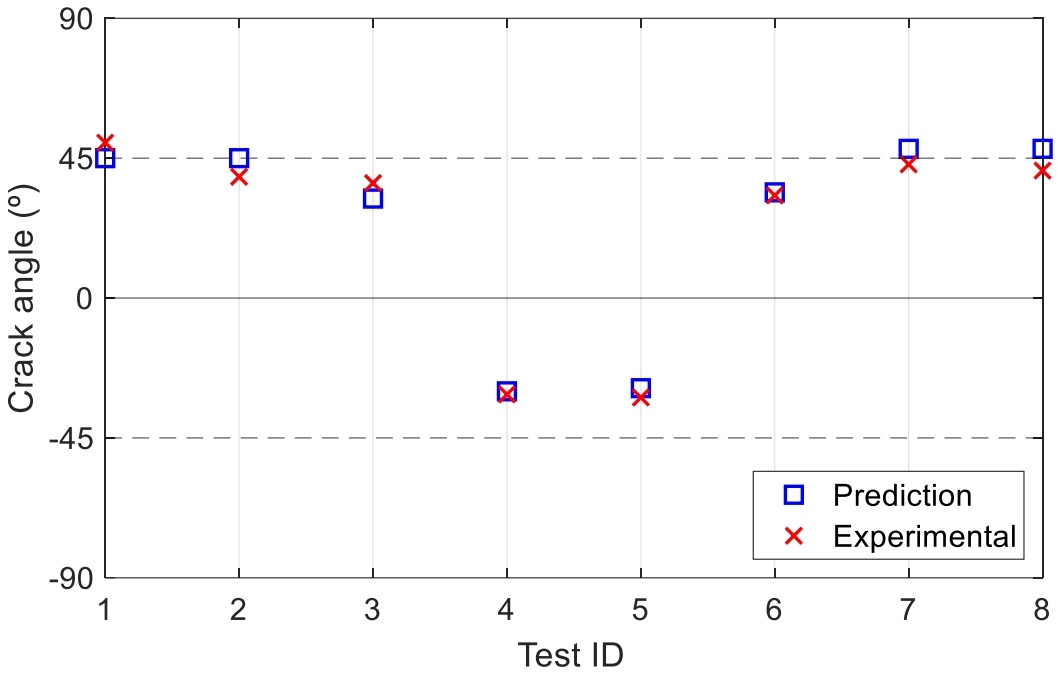

Figure 4.11 - Correlation between the measured critical plane and the estimated critical plane.

4.3.4. Observation of fracture surface

The fracture surface of the specimen subjected to fully reversed loading (σ_a = 200 MPa, N_f = 310,937 cycles) was observed by scanning electron microscopy (SEM). Three distinct regions can be identified, as shown in Fig. 4.12. Region A is characterized by small crack growth around the defect. Region B corresponds to the phase of long crack growth and is followed by region C, where the fast fracture occurs. A zoom in region A (Fig. 4.13) improves the visibility of the marks of small cracks and shows that fatigue cracks emanate around the defect, but identifying the exact site where the crack initiates is not easy. Figure 4.14 shows a zoom in region B, which is the crack propagation zone. As expected, it is possible to observe the fatigue striations. Lastly, Fig 4.15 is a zoom of region C and shows the dimples.

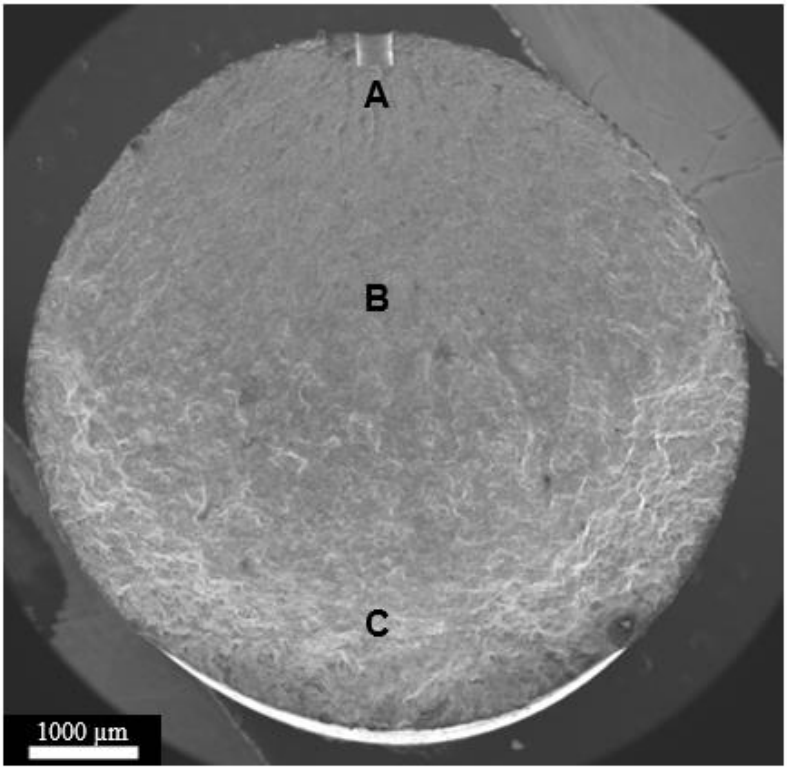

Figure 4.12 - SEM image of the fracture surface for the test subjected to tension-compression loading (σ_{xa} = 200 MPa, N_f = 310,937 cycles).

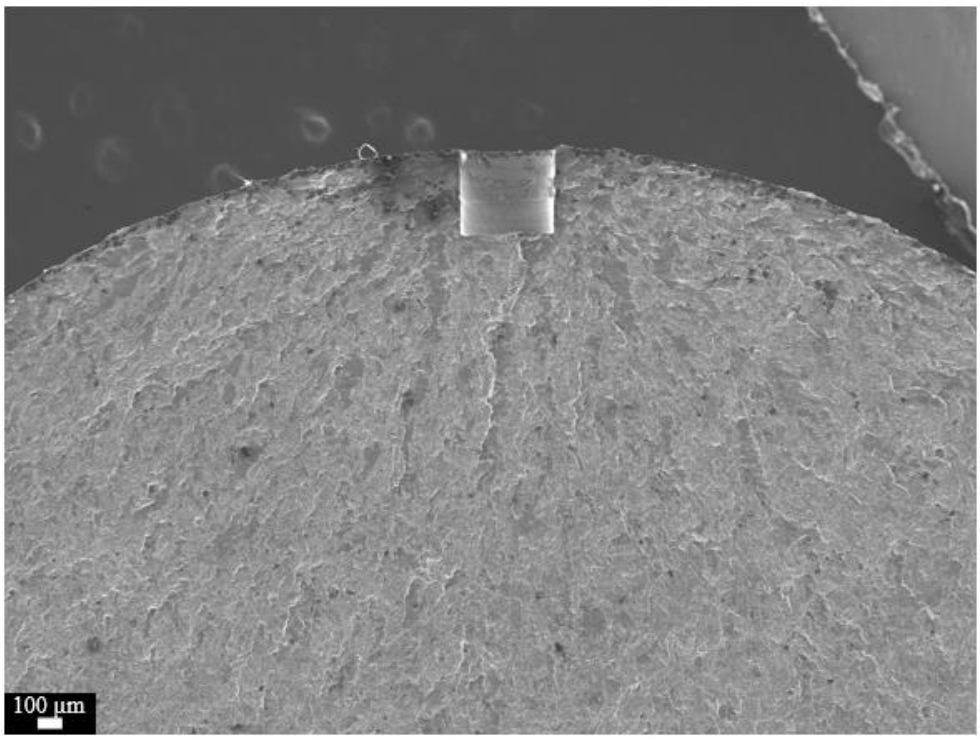

Figure 4.13 - SEM image of the fracture surface near the defect for the test subjected to tension-compression loading (σ_{xa} = 200 MPa, N_f = 310,937 cycles).

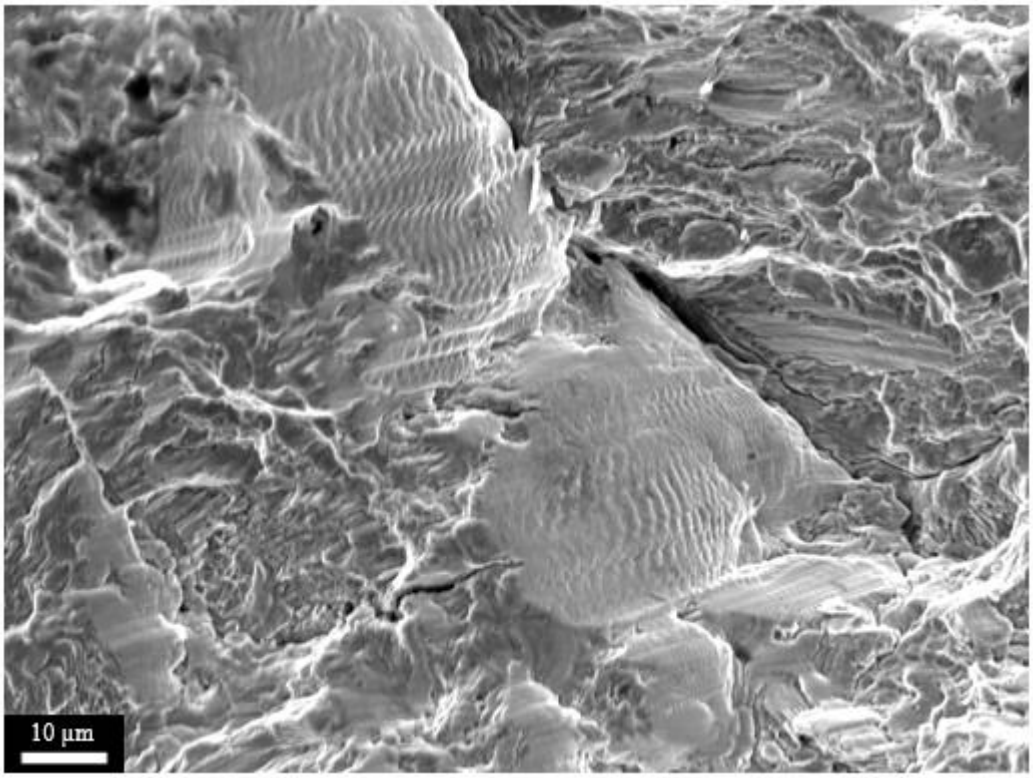

Figure 4.14 - SEM image of the crack propagation zone for the test subjected to tension-compression loading (σ_{xa} = 200 MPa, N_f = 310,937 cycles).

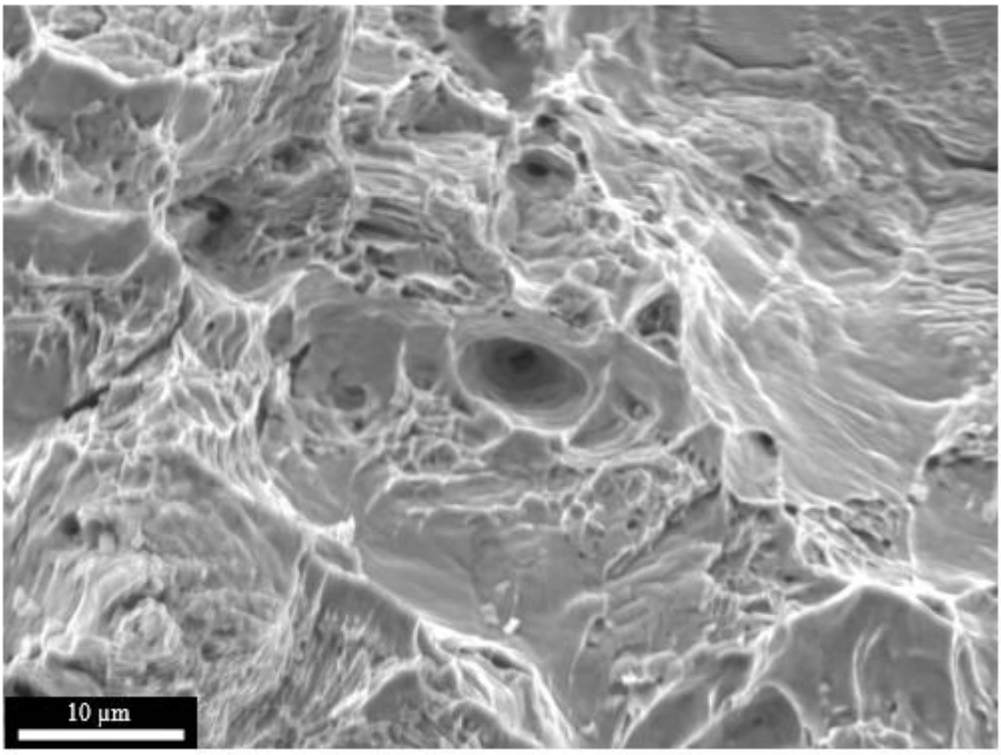

Figure 4.15 - SEM image of the fast fracture zone for the test subjected to tension-compression loading (σ_{xa} = 200 MPa, N_f = 310,937 cycles).

5. CONCLUSIONS

This work investigated the behavior of small fatigue cracks emanating from an artificial cylindrical defect in 1045 steel and evaluated the accuracy of small crack growth models in predicting fatigue life. The calibration of the models was made using small crack growth data obtained from uniaxial fatigue tests under stress ratios of -1 and 0.1. The small crack growth models were then applied to fatigue tests conducted under uniaxial, torsional, and axial/torsional loading conditions. The main conclusions of the work are listed below:

(1) The small crack growth model based on the SWT fatigue parameter correlated well with experimental data for uniaxial, torsional, and axial/torsional out-of-phase tests. However, the model is conservative for experiments conducted under uniaxial loading and axial/torsional in-phase loading, both with the presence of mean stress. For these cases, the difference between the estimated lives and the measured lives was up to a factor of 10.

(2) The proposed modification of the Fatemi model, which relies on a Walker-type parameter, significantly improved the life estimates of tests with the presence of mean stress. Most of the life estimates provided by the model were within a factor of 3 concerning the measured lives.

Although the model proposed here has been evaluated under some complex loading conditions, future research could assess its accuracy in predicting the fatigue life of other materials under different loading conditions. Also, studies dedicated to improving crack growth monitoring using, for example, digital image correlation, would be useful.

REFERENCES

[1] U. Zerbst, C. Klinger, R. Clegg, Fracture mechanics as a tool in failure analysis - Prospects and limitations, Eng. Fail. Anal. 55 (2015) 376–410. https://doi.org/10.1016/j.engfailanal.2015.07.001.

[2] U. Zerbst, M. Madia, C. Klinger, D. Bettge, Y. Murakami, Defects as a root cause of fatigue failure of metallic components. I: Basic aspects, Eng. Fail. Anal. 97 (2019) 777–792. https://doi.org/10.1016/j.engfailanal.2019.01.055.

[3] J. Lankford, S.J. Hudak r., Relevance of the small crack problem to lifetime prediction in gas turbines, Int. J. Fatigue. 2 (1987) 87–93.

[4] T. Shiraiwa, F. Briffod, M. Enoki, Prediction of Fatigue Crack Initiation of 7075 Aluminum Alloy by Crystal Plasticity Simulation, Materials (Basel). 16 (2023). https://doi.org/10.3390/ma16041595.

[5] A. Fatemi, A. Nourian-Avval, Fatigue life prediction of cast aluminum alloy based on porosity characteristics, Theor. Appl. Fract. Mech. 109 (2020) 102774. https://doi.org/10.1016/j.tafmec.2020.102774.

[6] S. Ye, C.C. Zhang, P.Y. Zhang, X.C. Zhang, S.T. Tu, R.Z. Wang, Fatigue life prediction of nickel-based GH4169 alloy on the basis of a multi-scale crack propagation approach, Eng. Fract. Mech. 199 (2018) 29–40. https://doi.org/10.1016/j.engfracmech.2018.05.023.

[7] Y. Murakami, T. Takagi, K. Wada, H. Matsunaga, Essential structure of S-N curve: Prediction of fatigue life and fatigue limit of defective materials and nature of scatter, Int. J. Fatigue. 146 (2021). https://doi.org/10.1016/j.ijfatigue.2020.106138.

[8] B. Wang, L. Xie, J. Song, X. He, W. Luo, B. Zhao, T. Mu, Failure behavior of aerial bomb lifting lug under variable amplitude loading: Failure analysis and life prediction, Eng. Fail. Anal. 120 (2021) 105000. https://doi.org/10.1016/j.engfailanal.2020.105000.

[9] A. Fatemi, A. Nourian-Avval, Fatigue performance and life prediction of cast aluminum under axial, torsion, and multiaxial loadings, Theor. Appl. Fract. Mech. 111 (2021) 1–12. https://doi.org/10.1016/j.tafmec.2020.102842.

[10] R.A. Costa, Influência de microdefeitos no limite de fadiga do aço 1045 submetido a carregamento axial- torcional: Experimentos e modelagem, Universidade de Brasília, 2021.

[11] K.J. Miller, The two thresholds of fatigue behavior, Fatigue Fract. Eng. Mater. Struct. 16 (1993) 931–939. https://doi.org/https://doi.org/10.1111/j.1460-2695.1993.tb00129.x.

[12] D.L. McDowell, V.P. Bennett, A microcrack growth law for multiaxial fatigue, Fatigue Fract. Eng. Mater. Struct. 19 (1996) 821–837.

[13] J. Schijve, Fatigue Crack Growth. Analysis and Predictions., in: Fatigue Struct. Mater., Springer, 2009: pp. 209–256. https://doi.org/https://doi.org/10.1007/978-1-4020-6808-9_8.

[14] Y. Jiang, M. Feng, Modeling of Fatigue Crack Propagation, J. Eng. Mater. Technol. 126 (2004) 77–86. https://doi.org/https://doi.org/10.1115/1.1631026.

[15] K.S. Chan, Roles of microstructure in fatigue crack initiation, Int. J. Fatigue. 32 (2010) 1428–1447. https://doi.org/10.1016/j.ijfatigue.2009.10.005.

[16] M.D. Sangid, The physics of fatigue crack initiation, Int. J. Fatigue. 57 (2013) 58–72. https://doi.org/10.1016/j.ijfatigue.2012.10.009.

[17] J. Schijve, Significance of Fatigue Cracks in Micro-Range and Macro-Range, ASTM STP. 415 (1967) 415–459. https://doi.org/10.1520/stp47238s.

[18] H. Kitagawa, S. Takahashi, Applicability of fracture mechanics to very small cracks or the cracks in the early stage, in: Int. Conf. Mech. Behav. Mater. 2nd 760816, 1976: pp. 627–631.

[19] H. Nisitani, M. Goto, A Small-Crack Growth Law and its Application to the Evaluation of Fatigue Life, Life. (1986) 461–478.

[20] D. Davidson, K. Chan, R. McClung, S. Hudak, Small Fatigue Cracks, in: Compr. Struct. Integr., 2003: pp. 129–164. https://doi.org/10.1016/B0-08-043749-4/04073-8.

[21] H. Nisitani, M. Goto, N. Kawagoishi, A small-crack growth law and its related phenomena, Eng. Fract. Mech. 41 (1992) 499–513. https://doi.org/10.1016/0013-7944(92)90297-R.

[22] H. Nishitani, N. Kawagoishi, Fatigue Crack Growth Laws in Small and Large Cracks and Their Physical Background, Chem. Pharm. Bull. 35 (1992) 1–11.

[23] N. Kawagoishi, Q. Chen, H. Nisitani, Significance of the small crack growth law and its practical application, Metall. Mater. Trans. A Phys. Metall. Mater. Sci. 31 (2000). https://doi.org/10.1007/s11661-000-0228-6.

[24] M. Goto, H. Nisitani, Fatigue Life Prediction of Heat-Treated Carbon Steels and Low Alloy Steels Based on a Small Crack Growth Law, Fatigue Fract. Eng. Mater. Struct. 17 (1994) 171–185. https://doi.org/10.1111/j.1460-2695.1994.tb00799.x.

[25] M.J.. Caton, J.W. Jones, J.E. Allison, Use of Small Fatigue Crack Growth Analysis in Predicting the S-N Response of Cast Aluminum Alloys, ASTM STP. 1372 (2000) 285–303.

[26] P.C. Paris, M.P. Gomez, W.E. Anderson, A Rational Analytical Theory of Fatigue, Trend Eng. 13 (1961).

[27] P.C. Paris, F. Erdogan, A Critical Analysis of Crack Propagation Laws, J. Basic Eng. 85 (1963) 528–533. https://doi.org/https://doi.org/10.1115/1.3656900.

[28] S. Pearson, Initiation of fatigue cracks in commercial aluminum alloys and the subsequent propagation of very short cracks, Eng. Fract. Mech. 7 (1975). https://doi.org/10.1016/0013-7944(75)90004-1.

[29] R.O. Ritchie, J. Lankford, Small fatigue cracks: A statement of the problem and potential solutions, Mater. Sci. Eng. 84 (1986) 11–16. https://doi.org/10.1016/0025-5416(86)90217-X.

[30] A. Shyam, J.E. Allison, J.W. Jones, A small fatigue crack growth relationship and its application to cast aluminum, Acta Mater. 53 (2005) 1499–1509. https://doi.org/10.1016/j.actamat.2004.12.004.

[31] N. Shamsaei, A. Fatemi, Small fatigue crack growth under multiaxial stresses, Int. J. Fatigue. 58 (2014) 126–135. https://doi.org/10.1016/j.ijfatigue.2013.02.002.

[32] P. Smith, K.N., Topper, T.H., Watson, A stress-strain function for the fatigue of metals (stress-strain function for metal fatigue including mean stress effect), J Mater. 5 (1970) 767–778.

[33] K. Walker, The effect of stress ratio during crack propagation and fatigue for 2024-T3 and 7075-T6 aluminum. Effects of Environment and Complex Load History on Fatigue Life, ASTM STP. 462 (1970) 1–14.

[34] T. Billaudeau, Y. Nadot, G. Bezine, Multiaxial fatigue limit for defective materials: Mechanisms and experiments, Acta Mater. 52 (2004) 3911–3920. https://doi.org/10.1016/j.actamat.2004.05.006.

[35] M. Endo, I. Ishimoto, Effects of Phase Difference and Mean Stress on the Fatigue Strength of Small-Hole-Containing Specimens Subjected to Combined Load, J. Solid Mech. Mater. Eng. 1 (2007) 343–354. https://doi.org/10.1299/jmmp.1.343.

[36] M. Endo, I. Ishimoto, The fatigue strength of steels containing small holes under out-of-phase combined loading, Int. J. Fatigue. 28 (2006) 592–597. https://doi.org/10.1016/j.ijfatigue.2005.05.013.

[37] F.C. Castro, E.N. Mamiya, C. Bemfica, A critical plane criterion to multiaxial fatigue of metals containing small defects, J. Brazilian Soc. Mech. Sci. Eng. 43 (2021) 1–15. https://doi.org/10.1007/s40430-021-03246-4.

[38] D. Socie, G. Marquis, Multiaxial fatigue, SAE International, 1999.

[39] ASTM, Standard Test Methods for Vickers Hardness and Knoop Hardness of Metallic Materials, (2018). https://doi.org/10.1520/E0092-17.2.

[40] ASTM, Standard Test Methods for Determining Average Grain Size, (2010) 1–27. https://doi.org/10.1520/E0112-13.1.4.

[41] ASTM, Standard Practice for Conducting Force Controlled Constant Amplitude Axial Fatigue Tests of Metallic Materials, (2021). https://doi.org/10.1520/E0466-21.2.

[42] ASTM, Standard Test Method for Measurement of Fatigue Crack Growth Rates, (2023). https://doi.org/10.1520/E0647-23.

[43] A.L. Dias, Influence of small defects on the fatigue limit of 304L stainless steel: axial-torsional experiments and modeling, Universidade de Brasília, 2020.